

# Design conditions for waves and water levels using extreme value analysis with covariates

Graham Feld<sup>a</sup>, David Randell<sup>b</sup>, Emma Ross<sup>b</sup>, Philip Jonathan<sup>c,d,\*</sup>

<sup>a</sup>Shell UK, Aberdeen AB12 3FY, United Kingdom.

<sup>b</sup>Shell Global Solutions International BV, Amsterdam, The Netherlands.

<sup>c</sup>Shell Research Limited, London SE1 7NA, United Kingdom.

<sup>d</sup>Department of Mathematics and Statistics, Lancaster University LA1 4YW, United Kingdom.

---

## Abstract

This article presents a step-by-step procedure for estimation of the joint distribution of  $N$ -year maximum significant wave height, individual wave and crest heights, and total water level, accommodating the effects of directional and seasonal variation, surge and tide. The approach is based on non-stationary extreme value analysis of peaks over threshold incorporating careful uncertainty quantification, and is illustrated for a North Sea location using hindcast data. The article further provides a brief overview of the development of a regulatory framework for specification of design conditions for total water level over the past half century.

*Keywords:* metocean design, extreme, total extreme water level, non-stationary, uncertainty

---

## 1. Introduction

Extremes of wave height and total water level (TWL) are key parameters for the design of fixed platforms in the offshore environment. Previous papers (e.g. Feld et al. (2015), Randell et al. (2015)) have described an approach to non-stationary extreme value analysis (henceforth called “CEVA”, abbreviating “Covariate Extreme Value Analysis”) for estimating  $N$ -year maxima of significant wave height, individual wave and crest heights, taking into account the variation in seasonal and directional covariates. Waves that impact the topsides and supporting beams of offshore structures are particularly significant since they result in a rapid increase in loading with inundation level. Extremes of TWL, namely the combination of wave crest and still water level (SWL, itself the sum of tide and storm surge), can cause bigger loads still, and are often of greater importance to the structural engineer than crest height alone. This paper builds on the approach described in previous papers to also include SWL effects in a manner which is consistent with the wave modelling methodology and which preserves the relationships between waves, storm surge and tidal levels that are observed within storms.

The underlying approach to the estimation of the wave component of TWL is based upon modelling storm peak events on a directional-seasonal covariate domain, described in outline in Section 4. Whilst this approach captures the storm peaks appropriately, in order to determine the maximum TWL within each storm, it is necessary to model more than just the peak sea state. This is due

---

\*Corresponding author [philip.jonathan@shell.com](mailto:philip.jonathan@shell.com)

28 to both the random nature of large individual wave crests within sea states near to the peak and  
29 also to the characteristics of the inter-relationships between waves, tide and surge. Both of these  
30 effects may result in the highest water level during a storm occurring at a time of lower significant  
31 wave height ( $H_S$ ) but higher tide and/or surge.

32 In order to represent the total water level variability throughout a storm event, therefore, repre-  
33 sentative *storm trajectories* are derived which aim to capture the variability of all of the key wave  
34 (Section 5) and surge (Section 6) parameters as the storm develops both temporally and direction-  
35 ally. These trajectories can then be appropriately re-scaled in order to match the severity of storm  
36 peaks randomly selected from the fitted extremal model.

37 To estimate maximum TWL in a storm, all these modelling components, i.e. storm peak modelling,  
38 wave and surge storm trajectory selection and tidal variations, need to be brought together and  
39 combined with the short-term variability of individual crest heights. In this way, for each simulated  
40 sea state in each storm event, individual maximum crests are randomly sampled and added to  
41 appropriately selected surge and tidal level. This process, explained in Section 7, is then repeated  
42 for all randomly-simulated storms over the return period of interest. For each period of simulation  
43 the maximum TWL for each direction and day-of-year are retained. This allows extreme values of  
44 TWL for any season-direction combination to be subsequently extracted and these can then further  
45 be aggregated to derive all-year and omni-directional extremes in a statistically consistent manner.  
46 This final simulation is described in Section 8.

47 This modelling procedure allows all extremes that may be required for design and operational  
48 purposes to be derived in a single analysis. For example, seasonal criteria for installation activi-  
49 ties are readily available; or, a re-alignment of a structure during the design phase can be easily  
50 accommodated by simply aggregating across different sets of directional sectors.

51 Throughout this whole process, uncertainties are propagated into the estimated distribution of  
52 the  $N$ -year maximum TWL, using the methods described. These uncertainties are captured by  
53 using bootstrapping of the original storm peak data, a range of wave and surge storm trajectory  
54 shapes, different tidal phases, a range of extreme value thresholds, random sampling of  $H_S$ , and  
55 random sampling of individual crest heights.

## 56 2. Background

57 For the offshore environment, we assume that TWL is defined as the sum of individual crest, surge  
58 and tidal components. The importance of TWL has been explored particularly within two areas  
59 of study (a) coastal flooding and over-topping, and (b) wave impact on marine bottom-founded  
60 structures. In the first of these, annual maxima from long time series were traditionally used as  
61 the basis for extrapolating to long return periods but based on SWL, i.e. combined tide and surge.  
62 This approach means, however, that many significant surge events will be excluded if they happen  
63 to occur at low tide and it also does not make the best use of the available data since only a single  
64 event per year is included. The combined effects of decoupled tide and surge were modelled in  
65 Pugh and Vassie (1978) by the Joint Probability Method (JPM) where non- parametric probability  
66 distributions for both were derived and, assuming independence, recombined statistically to obtain  
67 the statistics of overall SWL. In order to extrapolate to longer return periods an empirically-selected  
68 log distribution was fitted to the tail of positive surges. The approach made better use of the data  
69 by using all hourly samples but in so doing introduced a data set which consisted of dependent  
70 samples. This introduced a bias into the estimate of the non-exceedance probability associated  
71 with given return periods.

72 Despite the shortcomings of the method it has been widely applied although the method was sub-  
73 sequently revised by Tawn (1992) to de-cluster the surge data into independent events, to smooth  
74 the observed magnitudes and to fit a more statistically-justified generalised Pareto distribution  
75 (GPD) to the tail of the surge distribution. An empirical approach for adjusting the surge distri-  
76 bution for different tidal levels was also presented for application to those shallow locations where  
77 this was relevant. Hawkes et al. (2002) proposed a joint model for water level, wave height, wave  
78 steepness and their dependence. An extension of the JPM for application to cases with more than  
79 two variables was described by Liu et al. (2010) in the “Direct JPM” in which a multi-dimensional  
80 histogram was set up to include wave run up in addition to tide and surge. In this approach the  
81 characteristics of dependence between the three were explicitly captured by using an empirical  
82 non-parametric method although the details used for extrapolation beyond the length of the data  
83 set are unclear. Shevchenko and Ivelskaya (2015) broadened and generalised the original JPM to  
84 include a description of seasonal variability in mean sea level within the tidal harmonics and used  
85 the Gumbel distribution to extrapolate both surge and tsunami levels to longer return periods.  
86 However, any joint probability characteristics between the parameters were not explicitly modelled  
87 in this approach.

88 More sophisticated modelling approaches to joint probability in general have been developed by  
89 Heffernan and Tawn (2004) which describe the relationship of variable  $Y$  conditional on the value  
90 of another extreme variable  $X$  following transformation to a standard (typically Laplace) marginal  
91 scale

$$Y| \{X = x\} = ax + x^b W \quad (1)$$

92 where  $a \in [-1, 1]$  and  $b \in (-\infty, 1]$  are fitted parameters and  $W$  represents a residual process with  
93 unknown distribution, assumed Gaussian for fitting only. Typically a generalised Pareto distribu-  
94 tion (GPD) is used to fit each marginal distribution of peaks over threshold. The approach can  
95 be extended to any number of variables in which each is conditional upon the value of a single  
96 conditioning variable that exceeds a certain extremal threshold. Gouldby et al. (2014) applied this  
97 approach to the study of coastal over-topping and overflow which included SWL and wave compo-  
98 nents. Once the model was fitted, a Monte Carlo approach was used in which a single parameter  
99 was sampled randomly and the relationship presented above was used (including sampling from the  
100 distribution of residuals,  $W$ ) to determine associated values of other parameters in order to model  
101 for long return periods.

102 In terms of setting the deck height of offshore structures and the determination of extreme TWL  
103 in the North Sea, the design recipe in the 1970s and early 80s was based on a 1.5m clearance over  
104 and above a combination of the 50-year crest height, the 50-year surge and the mean high water  
105 spring (MHWS) tide (UK HMSO 1974). During the 1980s, the key return period was increased to  
106 100 years and some simple allowance was given for joint probabilities between tide and surge on the  
107 assumption of two Gaussian parameters between which a correlation coefficient could be defined  
108 (UK Department of Energy 1990).

109 By 1998, the UK Health and Safety Executive dictated that a structure needed to withstand the  
110 10,000-year TWL with no additional air gap but no clear guidance was given as to how the TWL  
111 should be derived. At this time, therefore, certain empirical methods were developed within the  
112 industry based on empirically-derived relationships founded on considerations such as storm length  
113 versus length of tidal cycle and rules of thumb relating crest heights from one return period to  
114 another. One such method for the 10,000-year TWL,  $TWL_{10000}$ , which was adopted by Shell and

115 BP in 2000 was the so-called “Interim method”

$$\text{TWL}_{10000} = C_{10000} + \frac{3}{4}(\text{MHW} - \text{MSL}) + S_1^+ \quad (2)$$

116 where MHW is the mean tidal high water,  $S_1^+$  is the 1-year positive surge,  $C_{10000}$  is the 1,000-year  
117 crest height, and MSL is mean sea level. A second approach was described in Leggett et al. (2007)  
118 for the central (CNS) and southern (SNS) North Sea

$$\begin{aligned} \text{CNS:} \quad & \text{TWL}_{10000} = C_{10000} + \text{MSL} + S_1^+ \\ \text{SNS:} \quad & \text{TWL}_{10000} = C_{10000} + \text{MSL} + S_3^+ \end{aligned} \quad (3)$$

119 where  $S_3^+$  is the 3-year positive surge, and where subscript 10000 refers to the 10,000-year value  
120 of the corresponding quantities; however this approach - based on consideration of only selected  
121 combinations of crest height, tide and surge rather than a general investigation of the worst possible  
122 combinations - was not generically applicable.

123 ISO19902 (2007) presented a range of TWL values for an offshore location utilizing relationships  
124 between tide, surge and crest and this was based on the approach set out by UK Department of  
125 Energy (1990). It provided limiting cases for TWL based on either complete correlation between  
126 surge and crest and the completely uncorrelated case. The range provided for TWL was

$$(\sqrt{a^2 + s^2 + t^2}, \sqrt{(a + s)^2 + t^2}) \quad (4)$$

127 where  $a$  is the extreme crest height,  $s$  is the extreme surge and  $t$  is the maximum elevation of tide  
128 relative to mean sea level.

129 ISO19901-1 (2005) adopted the Tromans and Vanderschuren (1995) storm-based approach for the  
130 determination of individual wave and crest height return values based on the statistical combination  
131 of the long-term distribution of storm maxima with the short-term distribution of individual waves.  
132 This correctly accounts for the fact that the largest waves in a storm do not necessarily come from  
133 the most severe sea state and that the largest waves in a given return period do not necessarily  
134 come from the storms with the largest  $H_S$ . However, there was still no further guidance as to how  
135 to combine these crest heights with SWL variations.

136 In UK Health and Safety Executive (2009), a Monte Carlo approach was described to combine the  
137 approach of Tromans and Vanderschuren (1995) for individual wave crests with a representation  
138 of the joint probabilities of waves and surge. Again, though, a simplistic approach was adopted in  
139 which once a randomly-selected  $H_S$  was selected, the surge of the same percentile was associated  
140 with the sea state such that effectively, a perfect correlation was assumed between waves and surge,  
141 but a random tide was included. An additional empirical correction factor was then derived from  
142 measured data to correct for the degree of correlation.

143 We note the work of Callaghan et al. (2008), Serafin and Ruggiero (2014), Wahl et al. (2017)  
144 and others on simulating wave environments for estimation of erosion and over-topping. Previous  
145 papers by some of the current authors have developed the Monte Carlo approach (e.g. Ewans and  
146 Jonathan 2008, Feld et al. 2015) in which the approach of Tromans and Vanderschuren (1995) was  
147 adopted for the crests but which allowed for varying characteristics by season and direction in order  
148 to better capture the changing statistical populations through the year and by direction.

149 In order to derive TWL, however, a method for combining these crests with appropriate tides and  
150 surges is required, and this is the substance of the current paper.

151 **3. Example data set**

152 For illustrative purposes, a data set from a location in the western half of the Southern North  
153 Sea in a water depth of around 20m has been chosen. The water level data consisted of hourly  
154 measurements at an offshore platform between October 2006 and December 2016 and the wave  
155 data came from the NORA10 (Norwegian Reanalysis, 10km wave hindcast model, Reistad et al.  
156 2011) WAM (third generation prognostic wave model, WAMDI 1988) hindcast grid point closest  
157 to the measurement location and covered the same period. A representation of the distribution  
158 of  $H_S$  by season and direction is shown in Figure 1 showing the significance of the covariates in  
159 determining the severity of any particular season-direction combination. In this plot, all the data  
160 points are shown as grey dots and the storm peaks are shown as black dots. Direction is defined  
161 as the direction from which storms propagate, measured clockwise from North.

162 [Figure 1 about here.]

163 Tides were separated from storm surges by harmonic analysis (using `T_Tide` software, Pawlowicz  
164 et al. 2002) of hourly mean original water level data, with residual level referred to as surge.  
165 Figure 2(a) shows the variability of surge with season with black dots representing all the observed  
166 data points; again the seasonality is obvious. A similar plot is shown for tide in Figure 2(b) where  
167 the small equinoctial effect on tides can be seen. The relationship between tide and surge is shown  
168 in Figure 2(c) in which the relationship appears to be random in nature in an overall sense, although  
169 there appears to be a slight tendency for the highest surges to have occurred at the extremes of  
170 tide either high or low. Figure 2(d) illustrates the overall relationship between  $H_S$  and surge. In  
171 this case, the largest surge events are associated with higher  $H_S$  values but the scatter indicates  
172 that a large  $H_S$  does not necessarily imply that a large surge will occur simultaneously.

173 [Figure 2 about here.]

174 For definiteness, wave height is defined as the difference between the maximum and minimum  
175 values of the ocean surface between consecutive down-crossings of mean water level. Crest height  
176 is defined as a the maximum value of the ocean surface between an up-crossing and subsequent  
177 down-crossing of the mean water level.

178 **4. Storm peak modelling**

179 The details of this approach have been described in previous papers (e.g. Feld et al. 2015). Briefly

180 1. A set of directional-seasonal covariate “bins” within which conditions are considered homoge-  
181 neous is defined. Binning reduces the computational complexity of the covariate description, and  
182 hence the complexity of the spline calculations to estimate extreme value (EV) models. Typi-  
183 cally, this is based on 32 directional bins ( $11.25^\circ$  width) and 24 seasonal bins (approximately 2  
184 weeks long) giving a total of 768 across the covariate domain.

185 2. A threshold  $q$  for isolation of storm event is defined using a quantile of sea state  $H_S$  per direction-  
186 season sector. This threshold is typically chosen to correspond to a quantile with constant  
187 non-exceedance probability of between approximately 0.5 and 0.75; this produces a sufficient  
188 number of storm events whilst keeping the storm length to a manageable size. A quantile is  
189 better than a fixed storm threshold since this ensures that calmer seasons and directions are

adequately represented in the overall model (and see e.g. Northrop and Jonathan 2011). The peak of the storm event is captured and characterised by the storm peak  $H_S$  (referred to as  $H_S^{sp}$  for definiteness where needed), zero-crossing wave period ( $T_Z$ ), spectral mean period,  $T_{01}$ , direction and day of year. Note that  $T_{01}$  is defined as  $\sqrt{m_0/m_1}$ , where  $m_0$  is the zero<sup>th</sup> moment and  $m_1$  the first moment of the wave spectrum;  $T_{01}$  is a key parameter in the Forristall crest height probability distribution.

3. For each storm, the whole period of exceedance of storm threshold  $q$  is also added to the set of historical storm trajectories which can then be associated with synthesized storm peaks (see Section 5).
4. A set of viable EV thresholds  $\psi$  for storm peaks was chosen, corresponding to quantiles with non-exceedance probabilities per covariate bin within some reasonable interval. Above  $\psi$ , occurrences of storm peaks are assumed to follow a Poisson process (with mean rate  $\rho$ ), and storm severity described by a generalised Pareto model (with scale parameter  $\sigma$  and shape parameter  $\xi$ ).
5. The variation of model parameters  $\psi$ ,  $\rho$ ,  $\sigma$  and  $\xi$  with covariates is described using linear combinations of cubic B-spline functions (or tensor products thereof) defined on the covariate domain. Each spline function has a fixed width but can vary in height. The extent to which spline function height is allowed to vary between adjacent splines is determined by penalty terms and an optimal smoothness chosen using cross-validated penalised maximum likelihood estimation. The intention is that spline smoothness is chosen so that the resulting variation in model parameters reflects the underlying natural variability present, whilst preventing overfitting. A conceptual illustration (unrelated to the current application) of the effect of high and low penalty cases is shown in Figure 3. In the left-hand case, the variability of heights between adjacent splines is much more constrained than the right-hand case. A penalised likelihood approach is also used to estimate covariate-dependent EV thresholds  $\psi$  in 4, above.
6. The procedure for partitioning the covariate domain is explained in (e.g.) Ross et al. (2017). We choose to partition the domain into 32 directional bins of width  $11.25^\circ$ , and 24 seasonal bins of width 15 *seasonal days* (from a year with 360 *seasonal days*). We judge this resolution to be sufficient to capture the main directional and seasonal variation of storm peak significant wave height. The extreme value model therefore uses a total of 768 ( $= 32 \times 24$ ) covariate combinations. For extreme value analysis we assume that neighbouring covariate bins exhibit similar behaviour. This is enforced by *penalising* the local variation of extreme value parameter estimates. We choose the penalty so that the resulting extreme value model has *optimal predictive performance*. In this sense, if there was no predictive evidence in the data related to covariate variation, the extreme value model would be extremely stiff, corresponding effectively to one covariate bin: in this case there would be one bin and 1156 peaks in it for the current application. Further, the *effective number* of covariate degrees of freedom used in the analysis can vary from one (stiff) to 768 (flexible). The actual effective number is chosen to maximise predictive performance using cross-validation. The optimal choice of parameter roughness penalty is discussed more fully in Section 6 and illustrated in Figure 6.

All modelling is performed for 768 covariate combinations. For presentation of results concerning the distribution of  $N$ -year maxima, we can combine covariate bins to present exactly the results that the engineer finds most useful. In this work, we present estimates (e.g. Figure 11 or Figure 12, discussed in Section 8) on 8 directional octants and 12 seasonal months. However,

233 we can provide estimates of extreme environments using any combinations of covariate bins of  
 234 interest to the engineer.

235 [Figure 3 about here.]

236 Once the storm peak modelling has been completed, a Monte Carlo approach can then be used  
 237 to simulate a set of random storm peaks for any given return period that reflects the underlying  
 238 statistical characteristics of the data. To capture uncertainties in this process, the original data  
 239 can also be bootstrapped and the whole modelling process repeated.

## 240 5. Derivation of storm wave trajectory

241 It is not sufficient to just base the analysis on storm peaks. There are two main reasons for this:  
 242 (a) an extreme value of TWL in a given directional sector will not necessarily correspond to an  
 243 occurrence of storm peak  $H_S$  in the same directional sector; it may occur as the tail of a storm  
 244 that peaks in a different direction sector, and (b) when looking at large individual wave and crest  
 245 values, these may occur during sea states that are not at the peak of storms.

246 A consequence of this approach is that the largest observed values in each of the direction sectors  
 247 are not and should not be statistically independent. In practice, however, the data are used in the  
 248 design process as if they were independent and this means that there is some level of conservatism  
 249 in the directional extremes. In general, though, the level of dependence is small for bins of size  $45^\circ$   
 250 or larger and the biggest effect is on the least severe sectors. If only storm peaks were used to derive  
 251 extremes, though, the results would be non-conservative so, on balance, the approach described  
 252 here is preferred. Note that the effect is not an issue for seasonal *sector* since storm lengths are  
 253 much shorter than the lengths of normal seasonal definitions.

254 We now assume that trajectories of storms within the database being analysed are representative  
 255 of the range of storm shapes that may be seen. Clearly, storms of different severities and in different  
 256 seasons and directions may have different characteristics, so the challenge is to identify storms that  
 257 have peaks that are *closest* to each randomly-simulated storm peak. To identify these, the observed  
 258 storm histories are aggregated into a set of bins defined by the storm peak values of  $H_S$ , direction  
 259 and day of year. This is illustrated in Figure 4 where bins populated with storm peaks from the  
 260 observed data are indicated in blue.

261 [Figure 4 about here.]

262 For every randomly-selected storm peak with characteristics  $(H_S^{sp}, \text{Drc}^{sp}, \text{Ssn}^{sp})$ , indicated by a  
 263 red dot in the figure, a *distance*  $D$  is defined to the centre of every bin (with characteristics  
 264  $(H_{S_{bin}}^{sp}, \text{Drc}_{bin}^{sp}, \text{Ssn}_{bin}^{sp})$ ) for which data is available, namely

$$\begin{aligned}
 D^2 = & \frac{(H_S^{sp} - H_{S_{bin}}^{sp})^2}{\alpha_{H_S}^2} + \frac{(\text{Ssn}^{sp} - \text{Ssn}_{bin}^{sp})^2}{\alpha_{\text{Ssn}}^2} \\
 & + \frac{(\text{Drc}^{sp} - \text{Drc}_{bin}^{sp})^2}{\alpha_{\text{Drc}}^2}
 \end{aligned} \tag{5}$$

265 where superscript *sp* indicates storm peak values,  $H_S$  is significant wave height, Ssn is the day of  
 266 year, Drc is direction and the  $\alpha$ s are scaling factors selected for each variable.

267 The bin that is closest for the selected scaling factors (indicated by the green bin in the figure) is  
 268 then used as a source of *archetype* storms (and corresponding trajectories) for the storm peak in  
 269 question. The scaling factors  $\alpha_{H_S}$ ,  $\alpha_{\text{Ssn}}$  and  $\alpha_{\text{Drc}}$  can be adjusted in order to fine-tune the relative  
 270 importance of the three dimensions for the data set under investigation. The number of archetype  
 271 storms in each bin can also be adjusted. A large number of storms would produce a more varied  
 272 array of potential storm shapes, so capturing uncertainty in the storm trajectory, but if the number  
 273 is set too large then there will be storms that are less similar to the simulated storm peak that are  
 274 also randomly selected. Suitable values of the  $\alpha$  parameters are chosen by inspection of diagnostic  
 275 plots illustrating the performance of storm trajectory matching using a cross-validation procedure;  
 276 historical storms are withheld from the analysis in turn, and then used as test cases. We find  
 277 values of  $\alpha$  parameters yielding adequate matching to the storm trajectory for the withheld storms.  
 278 Typical values of the  $\alpha$  parameters are given in Feld et al. (2015).

279 Once the archetype populations have been established, the trajectories will be randomly selected  
 280 for association with randomly-simulated storm peaks. If the selected storm trajectory for some  
 281 archetype (labelled  $*$  for definiteness) has peak characteristics  $H_S^{sp*}$ ,  $\text{Drc}^{sp*}$  and  $\text{Ssn}^{sp*}$ , the storm  
 282 trajectory is then adjusted as follows for association with a storm peak with characteristics  $H_S^{sp}$ ,  
 283  $\text{Drc}^{sp}$ ,  $\text{Ssn}^{sp}$ , such that (a) all  $H_S$  values are scaled by the ratio of  $H_S^{sp}/H_S^{sp*}$ , (b) the whole storm  
 284 history directions are rotated by  $\text{Drc}^{sp} - \text{Drc}^{sp*}$  so that the archetype storm peak direction matches  
 285 that of the simulated storm peak, and (c) wave periods are scaled such that after scaling, the  
 286 sea-state steepness  $S = 2\pi H_S/(gT_2)$  at every time step does not change.

287 For further discussion of the storm wave trajectory matching procedure, please see Feld et al.  
 288 (2015).

## 289 6. Still water level modelling

290 For the determination of TWL, the joint relationship between wave crests, tide and surge needs to  
 291 be captured. Within the CEVA methodology, the same storm archetype approach that is used for  
 292 storm wave trajectories is also used to describe the development of surge through storm histories, as  
 293 outlined in Section 6.1. For locations where the water depth is sufficiently shallow that variations in  
 294 the water depth can have an effect on the sea states it is important to also capture the tidal variation  
 295 from that same storm. For deeper-water locations, just the storm surge needs to be available and  
 296 the tide can be randomly sampled. These tidal approaches are described in Section 6.2.

### 297 6.1. Surge modelling

298 Within the period of each storm, as characterised by the exceedance of  $H_S$  above storm threshold  
 299  $q$ , the storm surge is characterised by its maximum, minimum, median and range, i.e. the difference  
 300 between the maximum and minimum storm surge as illustrated in Figure 5.

301 [Figure 5 about here.]

302 Linear relationships are then developed between each of these characteristics and the storm peak  
 303  $H_S$  within each of the directional and seasonal bin combinations giving a total of 768 different  
 304 fits. The relationship is defined in terms of (a) a selectable quantile of storm peak  $H_S$  and the  
 305 corresponding median value of surge characteristic (together referred to as a *lock point* (with value  
 306  $H_S\text{Lock}$ ,  $\text{SurgeLock}$ ) and (b) the slope of a linear least-squares fit between the surge characteristic  
 307 and storm peak  $H_S$  (with value  $\text{Slope}$ ). The allowed rate of variability of  $\text{Slope}$  with direction and



308 season is set using a smoothing B-spline, optimised using cross-validation. For a given covariate  
 309 bin, the model takes the form

$$\text{Surge} = \text{Slope} \times (H_S - H_{S\text{Lock}}) + \text{SurgeLock}. \quad (6)$$

310 Estimation of cross-validation smoothness penalties for **Slope** (in the case of the surge maxima  
 311 variable) is illustrated in Figure 6. The figure shows lack-of-fit from the regression model as a  
 312 function of **Slope** smoothness. Red lines illustrate how well the regression model describes variation  
 313 present in the data as a function of **Slope** smoothness: as **Slope** becomes smoother (from left to  
 314 right) the quality of fit reduces. The black line illustrates how well the regression model is able  
 315 to *predict* unseen data: at optimum smoothness, the lack-of-predictive-fit is a minimum. This is a  
 316 classic bias-variance trade-off.

317 To illustrate for the case of surge maxima, Figure 7 shows the variability of storm peak  $H_S$  lock  
 318 point, slope and storm surge maximum lock point. Figure 8 shows 95% uncertainty intervals (UI)  
 319 for the range of 96 linear fits within each of 8 aggregated directional sectors for the illustrative  
 320 example for storm surge maximum, surge median and surge minimum characteristics. In these  
 321 plots, the grey dots represent all the observed combinations of  $H_S$  and surge whilst the coloured  
 322 dots represent the  $H_S$  and surge maximum pairs (blue),  $H_S$  and surge median pairs (yellow) and  
 323  $H_S$  and surge minimum pairs (red). Similar plots (not shown) were examined by month. The plots  
 324 show that in general there is a broadening of surge maximum and surge minimum as  $H_S$  increases  
 325 with surge median in general tending to increase more slowly. This is apparent in plots split both  
 326 by season and direction. It is also evident that as expected, there are more severe events that occur  
 327 in the winter months and that the south-east and east are calmer directions.

328 [Figure 6 about here.]

329 [Figure 7 about here.]

330 [Figure 8 about here.]

331 In order to capture the variability in the relationship between storm surge characteristics and  $H_S$ ,  
 332 the residuals of the linear regression relationships, i.e. the differences between observed relationships  
 333 and the line of best fit are also saved. These are then sampled randomly during the final Monte  
 334 Carlo analysis and applied to the regression relationship for each storm. Residuals from storm  
 335 surge characteristics were inspected by direction and season, and did not show obvious structure.  
 336 Residuals are re-sampled during simulation to ensure that the natural variability in relationships is  
 337 captured rather than collapsing everything onto a single regression relationship. Figure 9 illustrates  
 338 the overall performance of the regression model for the storm surge maximum characteristic.

339 [Figure 9 about here.]

340 For given simulated storm peak  $H_S$  value, we use Equation 6 above to calculate a surge maximum,  
 341 surge median, surge minimum and surge range for the simulated storm; these values are dependent  
 342 on the storm peak direction and season of the simulated storm peak event. We refer to these  
 343 as mxm, mdn, mnm and rng for clarity. We next adjust the matched archetype surge trajectory  
 344  $\{s_t^*\}$  say (which originally has different values  $\text{mxm}^*$ ,  $\text{mdn}^*$ ,  $\text{mnm}^*$  and  $\text{rng}^*$  for the surge maximum,  
 345 median, minimum and range) such that the adjusted archetype surge trajectory  $\{s_t\}$  has the desired  
 346 values corresponding to the simulated storm peak event. There are numerous possible approaches

347 to achieve this. Here we outline a simple linear scaling approach based on matching surge median,  
 348 surge maximum and surge minimum only. For  $s_t^* > \text{mdn}^*$ , define  $s_t$  such that

$$\frac{s_t - \text{mdn}}{\text{mxm} - \text{mdn}} = \frac{s_t^* - \text{mdn}^*}{\text{mxm}^* - \text{mdn}^*} \quad (7)$$

349 and when  $s_t^* \leq \text{mdn}^*$ , define  $s_t$  such that

$$\frac{\text{mdn} - s_t}{\text{mdn} - \text{mnm}} = \frac{\text{mdn}^* - s_t^*}{\text{mdn}^* - \text{mnm}^*} \quad (8)$$

## 350 6.2. Tidal modelling

351 When a random storm is simulated the waves and surge are sampled from the same archetype  
 352 storm, so retaining the relationship between these components. For shallower-water locations,  
 353 the tidal component itself is sampled from the same storm as the waves and surge, but the tidal  
 354 component is not re-scaled. In most hindcasts that are available, the effect of the variation in still  
 355 water level on  $H_S$  is not captured as they are run with a constant water depth. For this reason, it  
 356 is often better to use measured wave and water level records to establish the relationships between  
 357  $H_S$  and still water levels. An example of the impact of water level on the  $H_S$  time trace is shown  
 358 in Figure 10.

359 [Figure 10 about here.]

## 360 7. Simulation of TWL and related variables

361 To obtain a single realisation of maximum TWL (and its components) for a single storm, the  
 362 following procedure is used. We start by (a) simulating a storm peak direction and season (from  
 363 the Poisson rate model), and a storm peak  $H_S$  (from the extreme value model). Then (b) we select  
 364 a historical archetype storm trajectory (of sea-state  $H_S$  with direction and season in time, and  
 365 surge in time) with similar storm peak characteristics to the simulated storm peak (as described  
 366 in Section 5), and (c) rescale the storm trajectory (sea-state  $H_S$ ) characteristics (as described  
 367 in Section 5) so that they agree with the simulated storm peak. Then (d) we rescale the surge  
 368 trajectory (as described in Section 6). Next (e), we sample a random historical interval of tide to  
 369 associate with the storm. Then (f) we estimate the water depth for every sea state using the SWL  
 370 components of tide and surge, and the mean sea level above bed. Subsequently (g) we randomly  
 371 sample maximum individual crest heights for each sea state using probability distributions based  
 372 on the corresponding water depth (typically the Forristall distribution is used but this can be  
 373 modified to fit water depth or swell characteristics where appropriate). Then (h) we add crest,  
 374 surge and tide components per sea state to obtain TWL. Finally (i) the maximum value of TWL  
 375 (per directional-seasonal covariate bin) is saved for the realisation.

376 To obtain a single realisation of maximum TWL corresponding to a period of  $N$  years, we simply  
 377 simulate the appropriate (random) number of storm events for  $N$  years, and retain the maximum  
 378 value of TWL (per directional-seasonal covariate bin) over all events.

379 In this way, the distribution of  $N$ -year maximum TWL can therefore be estimated from multiple  
 380  $N$ -year simulations, for any combination of directional-seasonal covariate bins of interest (including  
 381 the combination of all covariate bins). Typically, to estimate the distribution of  $N$ -year maximum  
 382 TWL, at least 200 realisations of  $N$ -years of data are calculated so that the central characteristics

383 (e.g. mean, median, mode) of the distribution of the  $N$ -year maximum TWL are estimated reliably.  
384 In the current work, 300 realisations of  $N$  years were evaluated. To estimate extreme quantiles  
385 (e.g. the 95%ile) of the distribution of the  $N$ -year maximum TWL precisely, a larger number of  
386 realisations would be required.

387 We note in passing that the computational efficiency of naive numerical simulation can often be  
388 considerably improved using e.g. numerical integration (e.g. Ross et al. 2017), importance sampling  
389 or other more thoughtful *smarter simulation*.

## 390 8. Estimation of the distribution of the $N$ -year event

391 To estimate the distribution of the  $N$ -year maximum for quantities of interest, CEVA uses a Monte  
392 Carlo approach to simulate all storms in a return period of interest multiple times by (a) fitting the  
393 Poisson and GP model to  $n_B$  different bootstrap resamples of the original data, and (b) making  
394  $n_R$  realisations of TWL (and its components) the full return period of interest for each bootstrap.  
395 This produces  $n_B \times n_R$  different realisations of the return period of interest, where each version  
396 consists of multiple storms each of which are simulated as described in Section 7 and from which  
397 just the largest values of  $H_S$ , individual wave height ( $H$ ), individual crest height ( $C$ ) and TWL are  
398 stored for every season-direction bin. This allows a probability distribution to be developed for the  
399 maximum of each of these variables for a return period of interest. The distribution of the  $N$ -year  
400 maximum for each bin can then be summarised by the quantile with non-exceedance probability  
401  $1/e$  (i.e. the 37<sup>th</sup> percentile), which corresponds to the  $N$ -year return value for that bin in the  
402 absence of parameter uncertainty. Other quantiles of the distribution can also be used, e.g. to  
403 summarise the width of the distribution of the  $N$ -year maximum.

404 Aleatory (natural inherent) and epistemic (data and modelling) uncertainties are captured through-  
405 out the simulation process. Natural variability of storm peaks for a given environment, of storm  
406 trajectories given storm peak, of wave heights and crests given storm trajectory and of tide are all  
407 quantified. Modelling uncertainty due to a finite original sample and choice of EV threshold is also  
408 quantified. The resulting probability distribution implicitly reflects these uncertainties. Typically,  
409 for applications to estimation of extreme wave environments based on hindcasts or measurements,  
410 the aleatory uncertainty is the major contributor to the width of the distribution of the  $N$ -year  
411 maximum.

412 In the example used here, only 15 realisations of 20 bootstraps of the original sample were taken;  
413 that is, 300 simulations overall have been used to illustrate the methodology. Using these simula-  
414 tions, the overall fit of the  $H_S$  model to the data as split by direction and season and overall are  
415 shown in Figure 11 split by direction. A similar plot, split by season, was also inspected. This  
416 is quite a small number of realisations to estimate the whole distribution, and is reflected in the  
417 jagged nature of the modelled median and 95% UI (black) lines fitted to the observed data (red  
418 dots); as noted earlier however, 300 realisations is sufficient to estimate the central features (e.g.  
419 median) of the distribution. The red dashed lines represent the 95% UI range from across all boot-  
420 strap resamples. Using more realisations would make the tails smoother or, alternatively, numerical  
421 integration can also be used. The overall comparison is good with the tail corresponding to the  
422 original data being contained within the 95% UI for the tail simulated under the fitted model.  
423 Towards the top end of the data sets, the 95% UI associated with the (red) bootstrap re-sampled  
424 data narrows because the same data points are being re-sampled each time.

425

[Figure 11 about here.]

426 Similar plots are shown in Figure 12 for all storm sea states as opposed to just the storm peaks split  
427 by direction. Plots split by month are also available. Again the overall comparison is good although  
428 the storm lengths seem to be under-estimated by the approach since the number of modelled sea  
429 states (indicated by the number to the right of Md1 above each plot) are lower than the actual (Act)  
430 number of sea states. Nevertheless, the overall comparison of the probability distributions is good.

431 [Figure 12 about here.]

432 From the 300 simulations, the distribution of the maxima are shown in Figure 13 in which larger  
433 overall widths of the curves indicate a higher level of variability. The 37<sup>th</sup> percentile and median  
434 values are indicated by the dashed horizontal lines. The overall curves for the 37<sup>th</sup> percentile of  
435 the distribution of the  $N$ -year maxima for  $H_S$ ,  $C$  and TWL are shown in Figure 14 and Figure 15.

436 [Figure 13 about here.]

437 [Figure 14 about here.]

438 [Figure 15 about here.]

439 Figure 16 shows a comparison between the observed combinations of  $H_S$  and surge that were  
440 observed overall and in each direction sector overlaid by median and 95% UI shown as red lines.  
441 The equivalent modelled values are represented by the black lines. Agreement between observed  
442 (red) and simulated (black) curves is good in the body of the data, becoming more uncertain for  
443 large  $H_S$  where (a) there are fewer data and (b) there is greater spread in surge for given  $H_S$ . The  
444 differences in the relationships in each direction sector are quite clear with many sectors exhibiting  
445 an increasingly negative surge as storms become more severe, particularly from the South-East. The  
446 North-West and North on the other hand show a positive correlation between  $H_S$  and surge. These  
447 reflect the different storm tracks taken by storms which produce northerly as opposed to southerly  
448 or easterly winds at the site which will in turn affect the magnitude of the inverse barometric effect  
449 and the relative timing of the peak in surge and the  $H_S$  peak in the different storm types.

450 [Figure 16 about here.]

451 Estimates for the 37<sup>th</sup> percentile of the distribution of the  $N$ -year maximum for splits by direction  
452 are shown in Table 1 and Table 2 for wave crest and TWL, respectively. Equivalent tables for results  
453 split by month are shown in Table 4 and Table 5. Differences between TWL and crest values in  
454 the tables are termed *implied SWL* values and are given in Table 3 and Table 6 for values split by  
455 direction and season, respectively. We note that, for any  $N$ -year period, the implied SWL should  
456 be interpreted as the value of SWL that, when added to the 37th percentile of the distribution  
457 of  $N$ -year maximum of individual crest, provides the 37th percentile of the distribution of  $N$ -year  
458 maximum TWL. The term *implied SWL* is used since the largest TWL will not necessarily occur  
459 at the time of maximum individual crest height. This effect will become more significant at a  
460 location where the wave climate is not that severe and the tides are large. These tables show the  
461 varying level of contribution by direction sector as reflected in Figure 16. Overall, the implied SWL  
462 values are larger for the North and North-West sectors than for the other sectors albeit with some  
463 variability. This could be associated with noise due to insufficient realisations in the analysis or it  
464 may indicate a varying degree of association between the timing of maximum surge and maximum  
465 wave conditions across the directional-seasonal domain.

466 [Table 1 about here.]

467 [Table 2 about here.]

468 [Table 3 about here.]

469 [Table 4 about here.]

470 [Table 5 about here.]

471 [Table 6 about here.]

## 472 9. Discussion and conclusions

473 In addition to the derivation of extreme  $H_S$  and individual wave height, the covariate extreme value  
474 approach (CEVA) allows for the natural variability in waves and SWL and their joint probabilities  
475 to be modelled over long periods of time. This allows estimation of the joint distribution of  $N$ -year  
476 maxima of wave crest, storm surge and tide, and hence TWL. The approach includes the capability  
477 of reflecting the variability of climate with direction and season and also the correlation between  
478 the various components being studied in a non-parametric fashion which makes the approach very  
479 general.

480 There are some limitations to the approach, however, the main one being that sufficient storm  
481 events need to be available in the underlying data set in order to populate the many season-direction  
482 bins adequately at the start of the analysis. Where data sets are shorter, or fewer events occur  
483 per year (for example, for tropical cyclones) this can be a problem, but the analysis can be carried  
484 out in with just one covariate in this case (typically direction) to increase the number of events  
485 per underlying bin. However, this still may result in poor model fits if the data set is too small. A  
486 further difficulty of the approach is that in order to get statistically stable results a large number of  
487 realisations needs to be run and this can be time-consuming even with good computing resources.  
488 Using parallel processing is a significant help in this regard, but the end-point of the development  
489 is *smarter simulation* incorporating clever sampling, numerical integration and parallel processing  
490 rather than naive Monte Carlo analysis for long return periods. A further enhancement that is  
491 under development (Ross et al. 2018) for inclusion within CEVA is the use of the approach of  
492 Heffernan and Tawn (2004) to determine the associated surge characteristics rather than using  
493 the linear regression and residuals approach described here. It is also understood that the surge  
494 and wave trajectory re-scaling approaches are relatively crude and more sophisticated statistical  
495 approaches (e.g. Tendijck et al. 2018) are being developed to describe those more systematically.  
496 Despite the limitations described here, the overall approach has been shown to produce good results  
497 in several of the major oil and gas basins and allows the complexity of the environment to be well  
498 captured within a single analysis.

## 499 References

500 Callaghan, D., Nielsen, P., Short, A., Ranasinghe, R., 2008. Statistical simulation of wave climate  
501 and extreme beach erosion. *Coastal Engineering* 55 (5), 375 – 390.

- 502 Ewans, K. C., Jonathan, P., 2008. The effect of directionality on northern North Sea extreme wave  
503 design criteria. *J. Offshore. Arct. Eng.* 130, 041604:1–041604:8.
- 504 Feld, G., Randell, D., Wu, Y., Ewans, K., Jonathan, P., 2015. Estimation of storm peak and  
505 intra-storm directional-seasonal design conditions in the North Sea. *J. Offshore. Arct. Eng.* 137,  
506 021102:1–021102:15.
- 507 Gouldby, B., Mendez, F., Guanache, Y., Rueda, A., Minguez, R., 2014. A methodology for deriving  
508 extreme nearshore sea conditions for structural design and flood risk analysis. *Coastal Eng.* 88,  
509 15–26.
- 510 Hawkes, P. J., Gouldby, B. P., Tawn, J. A., Owen, M. W., 2002. The joint probability of waves and  
511 water levels in coastal defence design. *Journal of Hydraulic Research* 40, 241–251.
- 512 Heffernan, J. E., Tawn, J. A., 2004. A conditional approach for multivariate extreme values. *J. R.*  
513 *Statist. Soc. B* 66, 497–546.
- 514 ISO19901-1, 2005. Petroleum and natural gas industries. Specific requirements for offshore struc-  
515 tures. Part 1: Metocean design and operating considerations. First edition. International Stan-  
516 dards Organisation.
- 517 ISO19902, 2007. Petroleum and natural gas industries. Fixed offshore structures. First edition.  
518 International Standards Organisation.
- 519 Leggett, I. M., Bellamy, N. F., Fox, J. P., Sheikh, R., 2007. OMAE2007-29559: A recommended  
520 approach for deriving ISO-compliant 10,000 year extreme water levels in the North Sea. *Proc.*  
521 *26th Conf. Offshore Mech. Arct. Eng.*
- 522 Liu, J. C., Lence, B. J., Isaacson, M., 2010. Direct joint probability method for estimating extreme  
523 sea levels. *Journal of Waterway, Port, Coastal, and Ocean Engineering* 136, 66–76.
- 524 Northrop, P., Jonathan, P., 2011. Threshold modelling of spatially-dependent non-stationary ex-  
525 tremes with application to hurricane-induced wave heights. *Environmetrics* 22, 799–809.
- 526 Pawlowicz, R., Beardsley, B., Lentz, S., 2002. Classical tidal harmonic analysis including error  
527 estimates in MATLAB using TTIDE. *Computers and Geosciences* 28, 929–937.
- 528 Pugh, D., Vassie, J., 1978. Extreme sea levels from tide and surge probability. *Proc. 16th Coastal*  
529 *Engng Conf.* 1, 911–930.
- 530 Randell, D., Feld, G., Ewans, K., Jonathan, P., 2015. Distributions of return values for ocean  
531 wave characteristics in the South China Sea using directional-seasonal extreme value analysis.  
532 *Environmetrics* 26, 442–450.
- 533 Reistad, M., Breivik, O., Haakenstad, H., Aarnes, O. J., Furevik, B. R., Bidlot, J.-R., 2011. A high-  
534 resolution hindcast of wind and waves for the North sea, the Norwegian sea, and the Barents  
535 sea. *J. Geophys. Res.* 116, 1–18.
- 536 Ross, E., Randell, D., Ewans, K., Feld, G., Jonathan, P., 2017. Efficient estimation of return value  
537 distributions from non-stationary marginal extreme value models using Bayesian inference. *Ocean*  
538 *Eng.* 142, 315–328.

- 539 Ross, E., Sam, S., Randell, D., Feld, G., Jonathan, P., 2018. Estimating surge in extreme North  
540 Sea storms. *Ocean Eng.* 154, 430–444.
- 541 Serafin, K. A., Ruggiero, P., 2014. Simulating extreme total water levels using a time-dependent,  
542 extreme value approach. *Journal Geophys. Res. - Oceans* 119 (9), 6305–6329.
- 543 Shevchenko, G., Ivelskaya, T., 2015. Estimation of extreme sea levels for the russian coasts of the  
544 kuril islands and the sea of okhotsk. *Pure and Applied Geophysics* 172, 3537–3555.
- 545 Tawn, J. A., 1992. Estimating probabilities of extreme sea levels. *J. Roy. Statist. Soc. C* 41, 77–93.
- 546 Tendijck, S., Ross, E., Randell, D., Jonathan, P., 2018. A non-stationary statistical  
547 model for the evolution of extreme storm events. (Submitted to *Environmetrics*, draft at  
548 [www.lancs.ac.uk/~jonathan](http://www.lancs.ac.uk/~jonathan)).
- 549 Tromans, P. S., Vanderschuren, L., 1995. Variable based design conditions in the North Sea: ap-  
550 plication of a new method. *Offshore Technology Conference, Houston (OTC-7683)*.
- 551 UK Department of Energy, 1990. Metocean parameters - parameters other than waves. Supporting  
552 document to Offshore installations: guidance on design, construction and certification - environ-  
553 mental considerations (OTH 89 299). Her Majesty's Stationary Office (UK).
- 554 UK Health and Safety Executive, 2009. A Monte Carlo approach to joint probability of wave, tide  
555 and surge in extreme water level calculations (Research Report RR740). HSE Books (UK).
- 556 UK HMSO, 1974. The offshore installations (construction and survey) regulations (SI 174 / 289).  
557 Her Majesty's Stationary Office (UK).
- 558 Wahl, T., Haigh, I. D., Nicholls, R. J., Arns, A., Dangendorf, S., Hinkel, J., Slangen, A. B. A.,  
559 2017. Understanding extreme sea levels for broad-scale coastal impact and adaptation analysis.  
560 *Nat. Commun.* 8, 16075.
- 561 WAMDI, 1988. The WAM Model: A Third Generation Ocean Wave Prediction Model. *J. Phys.*  
562 *Oceanogr.* 18, 1775–1810.

563 **List of Figures**

564 1 Example data set: variation of  $H_S$  by direction (top) and season (bottom). Grey  
565 dots represents all data, black dots represent storm peaks. . . . . 18

566 2 Example data set: (a) surge on month, (b) tide on month, (c) surge versus tide, both  
567 with respect to long-term mean sea level, and (d) surge versus  $H_S$ . . . . . 19

568 3 Illustration of (a) high penalty spline combinations and (b) low penalty splines. The  
569 total representation of variability is indicated by the heavy black lines. . . . . 20

570 4 Representation of distance from a random storm peak at ( $H_{ssp}$ ,  $S_{nsp}$ ,  $D_{rcsp}$ ) to  
571 each direction-season bin ( $H_{sbin}$ ,  $S_{nbin}$ ,  $D_{rcbin}$ ). The bins which contain storms  
572 are indicated by the blue boxes. Each bin contains a population of storm trajectories  
573 which are randomly selected. The green bin is closest to the storm peak. . . . . 21

574 5 Storm surge characteristics and definitions. Panel (a) shows  $H_S$  in time with ver-  
575 tical black lines representing start and end of storm period. Panel (b) shows the  
576 corresponding surge time-series, with minimum, median and maximum values as  
577 horizontal dashed black lines. . . . . 22

578 6 Selection of optimal spline penalty coefficients for storm surge maximum. Red rep-  
579 represents lack of fit, black represents predictive performance. Minimum point of the  
580 black line represents the optimum penalty coefficient used for modelling. Similar  
581 plots are available for surge minimum, median and range. . . . . 23

582 7  $H_S^{sp}$  lock (left), slope (middle) and surge lock (right) for storm surge maximum.  
583 Similar plots are available for surge minimum, median and range. . . . . 24

584 8 95% uncertainty intervals for 96 linear fits within each directional sector of storm  
585 surge versus  $H_S$ . Surge maximum (blue), median (yellow) and minimum (red).  
586 Coloured points show surge maximum, median and minimum values; all other pairs  
587 are shown in grey. . . . . 25

588 9 Observed and predicted storm surge maxima with best-fit line shown. Similar plots  
589 are available for storm minima, storm median and storm range. . . . . 26

590 10 Time series of  $H_S$ , surge and tide for a shallow-water location (21.0m) showing the  
591 impact that tide can have on the variation in  $H_S$  through storms. . . . . 27

592 11 Comparison between resampled underlying data (red) and simulated (black) storm  
593 peaks for the overall case (left) and for each directional sector. Solid lines represent  
594 median case, dashed lines represent the 95% uncertainty intervals. The original data  
595 is shown as red dots. Similar plots are available resolved by month. . . . . 28

596 12 Comparison between resampled underlying data (red) and simulated (black) all  
597 storm sea-states for the overall case (left) and for each directional sector. Solid  
598 lines represent median case, dashed lines represent the 95% uncertainty intervals.  
599 The original data is shown as red dots. Similar plots are available resolved by month. 29

600 13 Distribution of the 10,000-year maximum of  $H_S$  (a) by direction and (b) by season.  
601 In each case, the overall *omni-covariate* curve is shown in black. . . . . 30

602 14 37<sup>th</sup> percentile of the distribution of  $N$ -year maximum  $H_S$  (a) by direction and (b)  
603 by season, by return period. The overall *omni-covariate* curve is shown in black. . . 31

604 15 37<sup>th</sup> percentile of the distribution for  $N$ -year maximum (a) wave crest by direction,  
605 (b) wave crest by season, (c) total water level by direction, and (d) total water level  
606 by season, as a function of return period. The overall *omni-covariate* curve is shown  
607 in black. . . . . 32



608 16 Comparison of observed (red) and simulated (black) median and 95% uncertainty  
609 intervals for storm surge versus  $H_S$ . Actual historical pairs of sea state  $H_S$  and  
610 surge are given as grey dots. . . . . 33

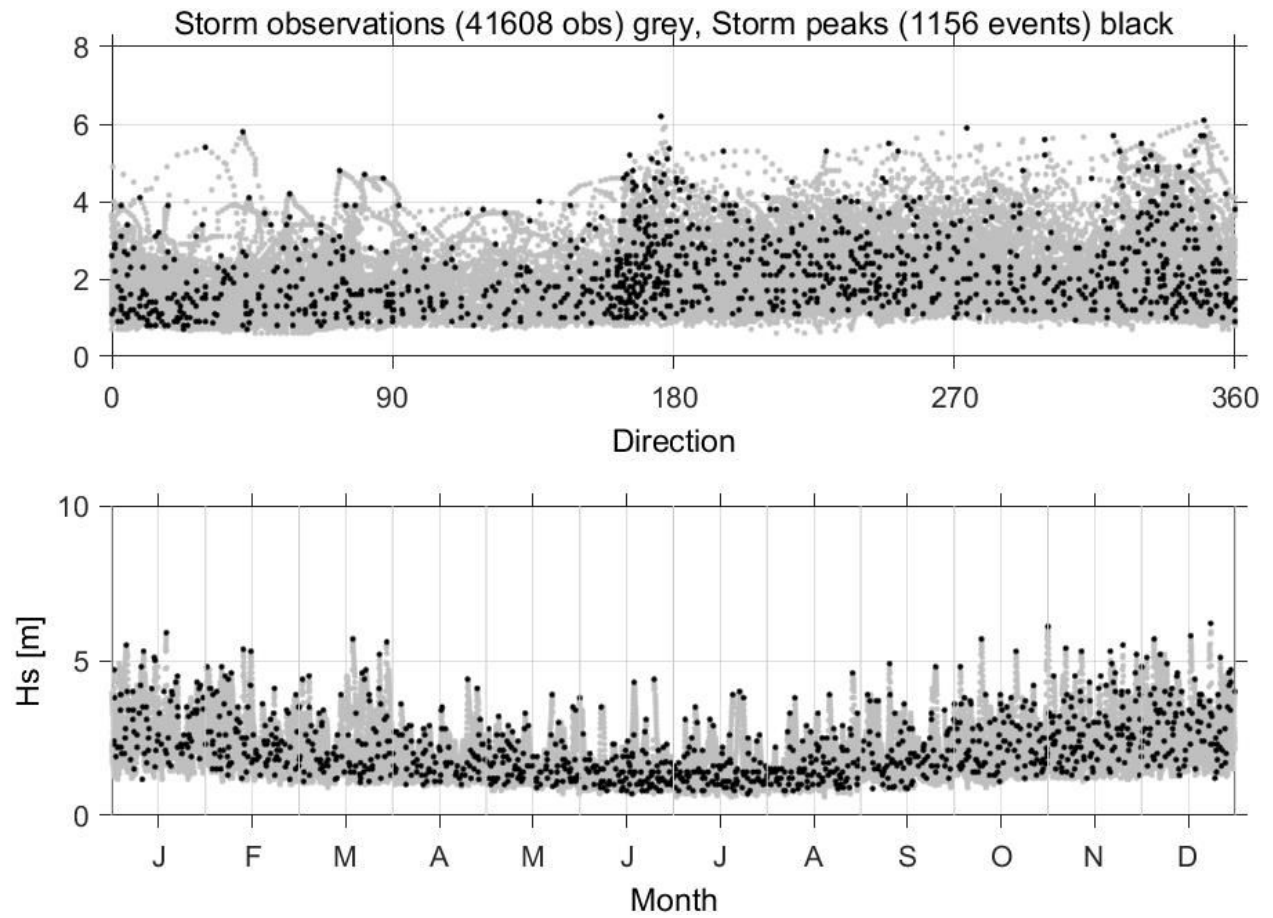


Figure 1: Example data set: variation of  $H_S$  by direction (top) and season (bottom). Grey dots represents all data, black dots represent storm peaks.

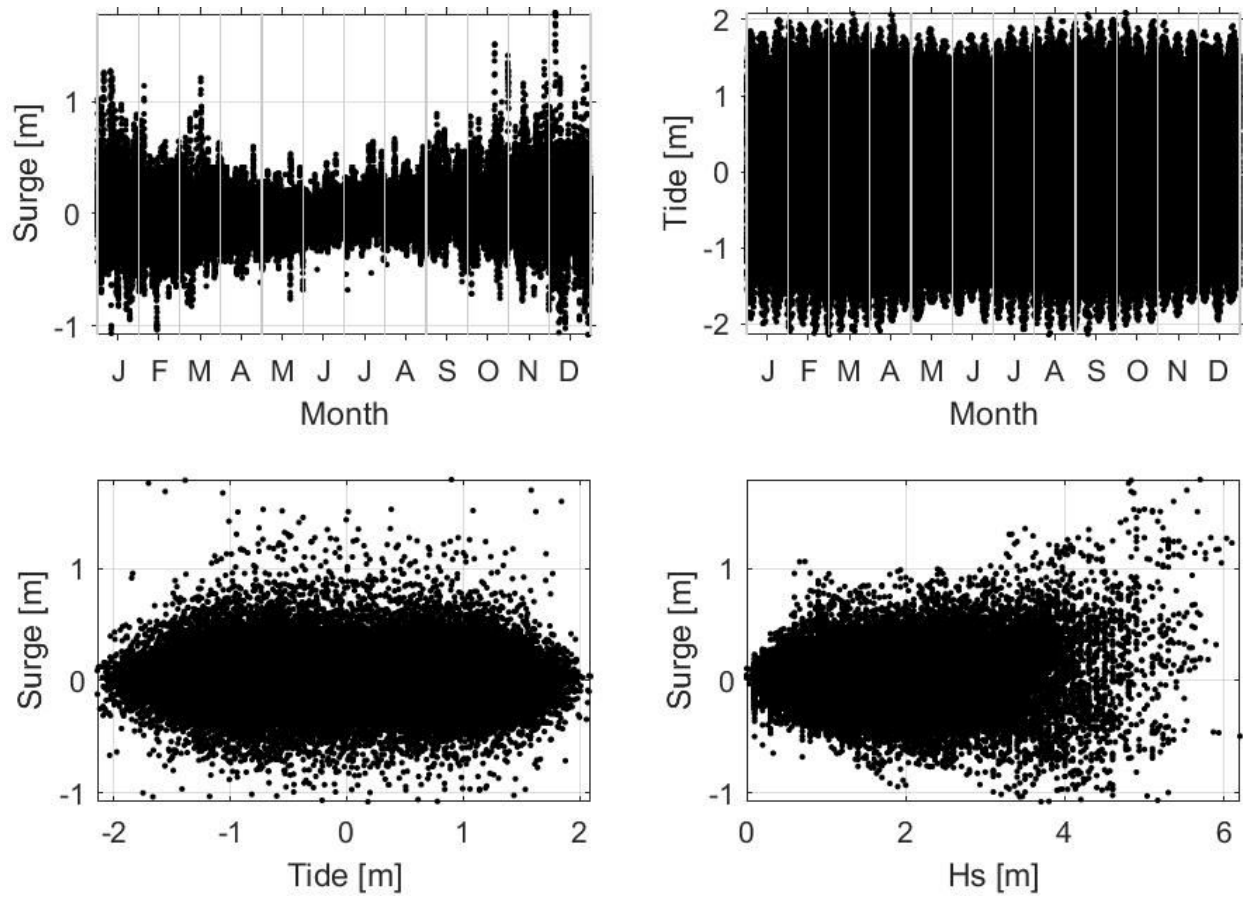


Figure 2: Example data set: (a) surge on month, (b) tide on month, (c) surge versus tide, both with respect to long-term mean sea level, and (d) surge versus  $H_s$ .

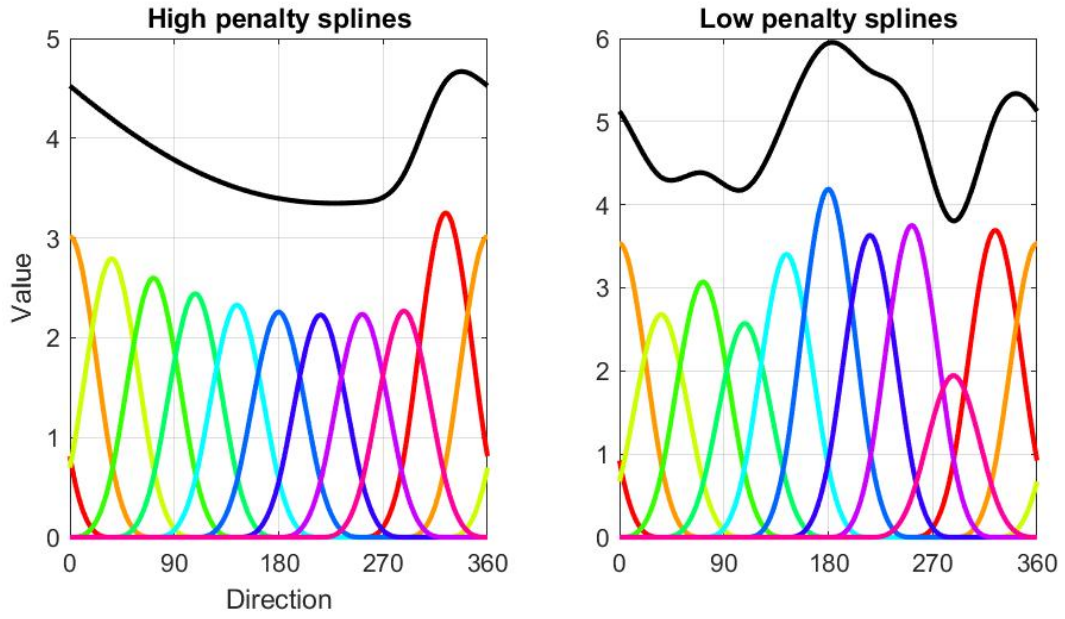


Figure 3: Illustration of (a) high penalty spline combinations and (b) low penalty splines. The total representation of variability is indicated by the heavy black lines.

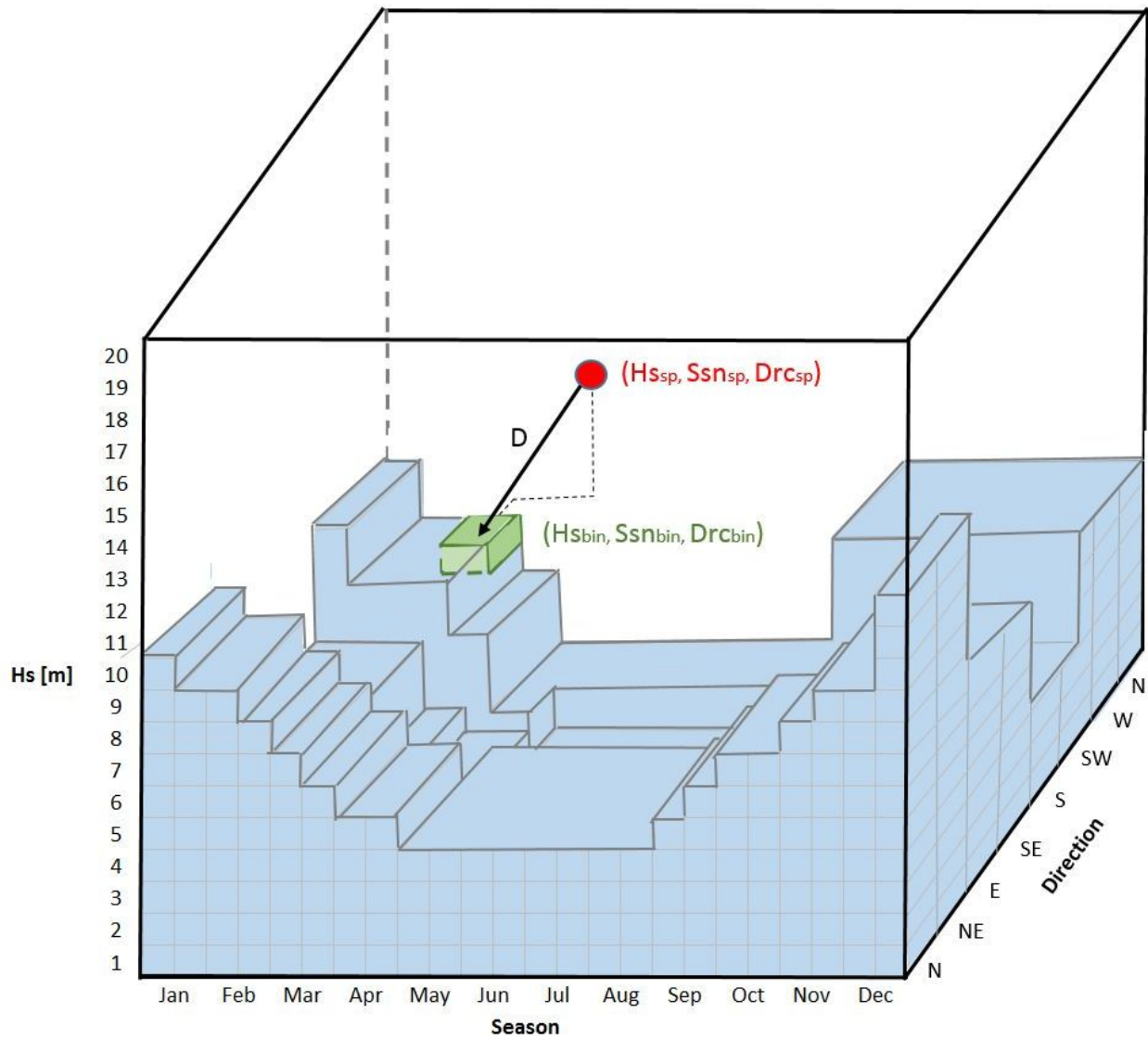


Figure 4: Representation of distance from a random storm peak at  $(Hs_{sp}, Ssn_{sp}, Drc_{sp})$  to each direction-season bin  $(Hs_{bin}, Ssn_{bin}, Drc_{bin})$ . The bins which contain storms are indicated by the blue boxes. Each bin contains a population of storm trajectories which are randomly selected. The green bin is closest to the storm peak.

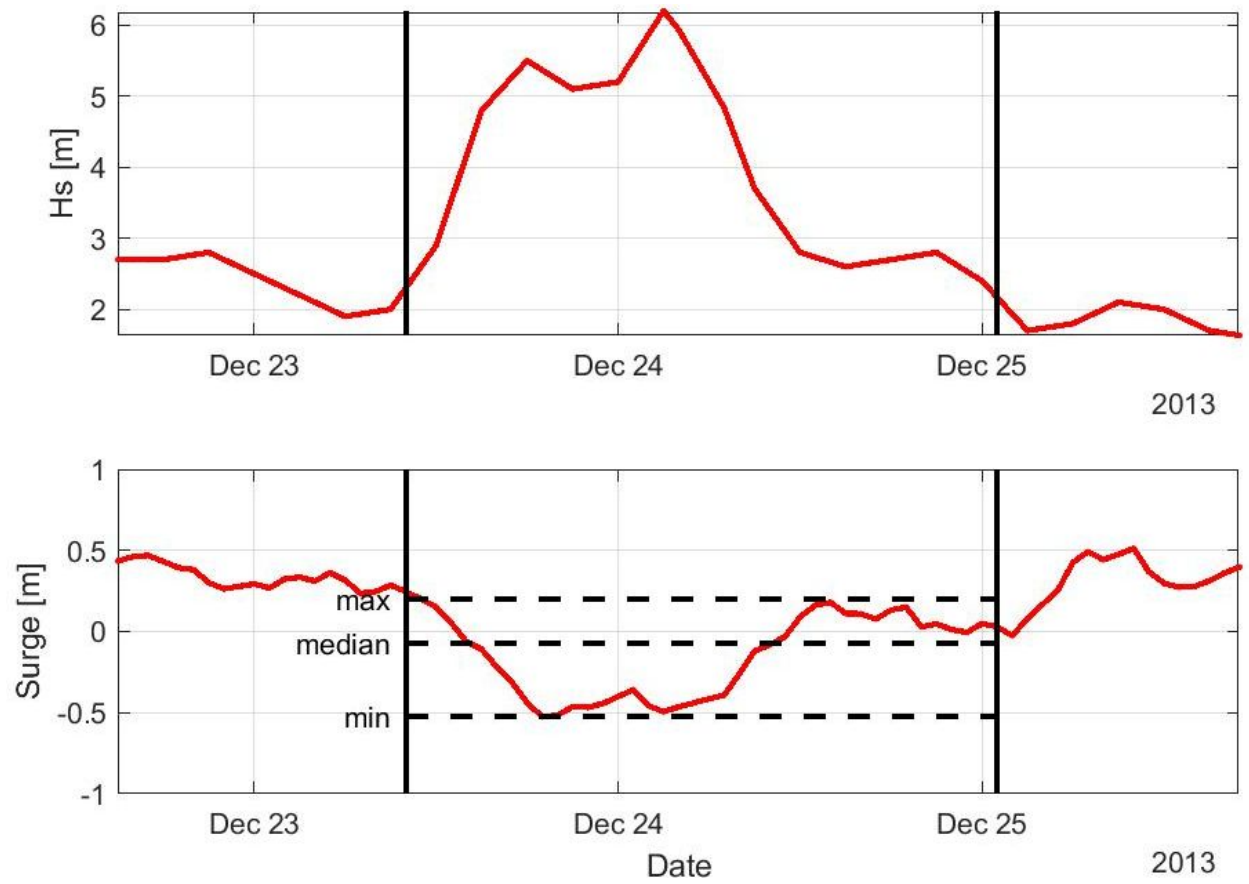


Figure 5: Storm surge characteristics and definitions. Panel (a) shows  $H_s$  in time with vertical black lines representing start and end of storm period. Panel (b) shows the corresponding surge time-series, with minimum, median and maximum values as horizontal dashed black lines.

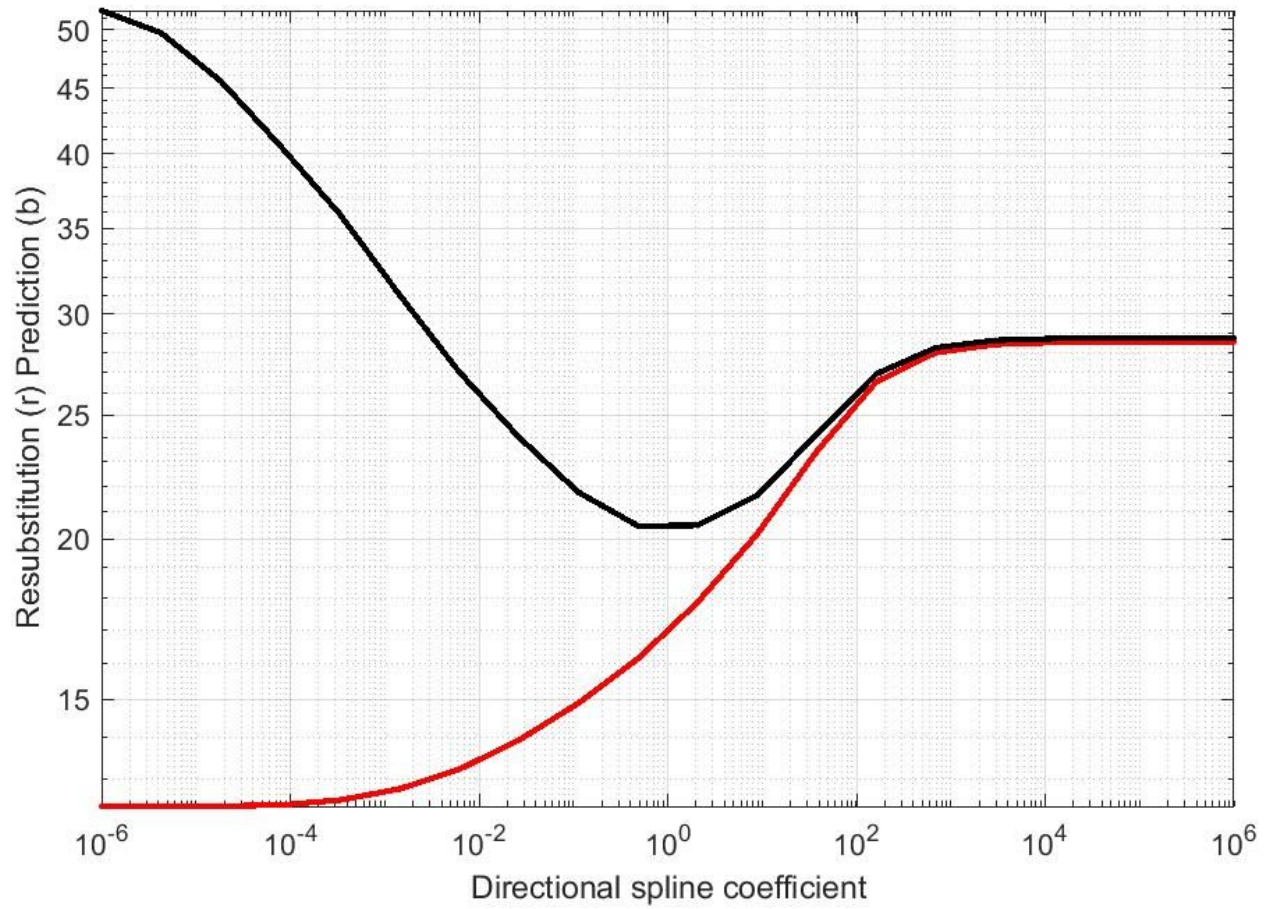


Figure 6: Selection of optimal spline penalty coefficients for storm surge maximum. Red represents lack of fit, black represents predictive performance. Minimum point of the black line represents the optimum penalty coefficient used for modelling. Similar plots are available for surge minimum, median and range.

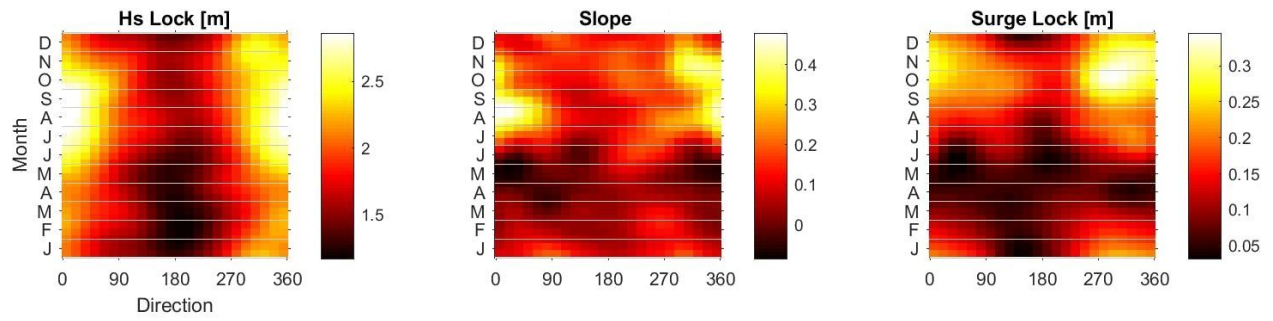


Figure 7:  $H_S^{sp}$  lock (left), slope (middle) and surge lock (right) for storm surge maximum. Similar plots are available for surge minimum, median and range.



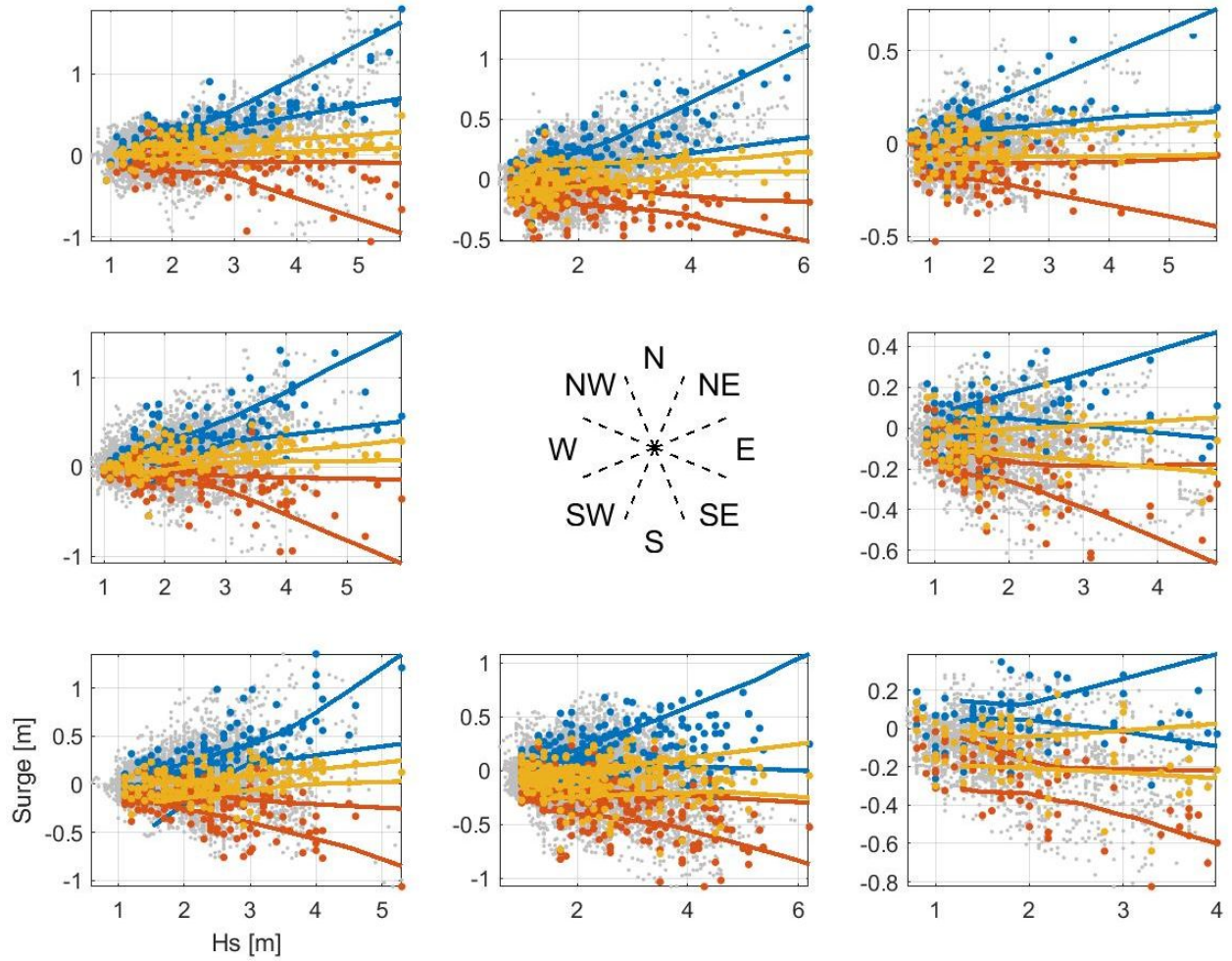


Figure 8: 95% uncertainty intervals for 96 linear fits within each directional sector of storm surge versus  $H_S$ . Surge maximum (blue), median (yellow) and minimum (red). Coloured points show surge maximum, median and minimum values; all other pairs are shown in grey.

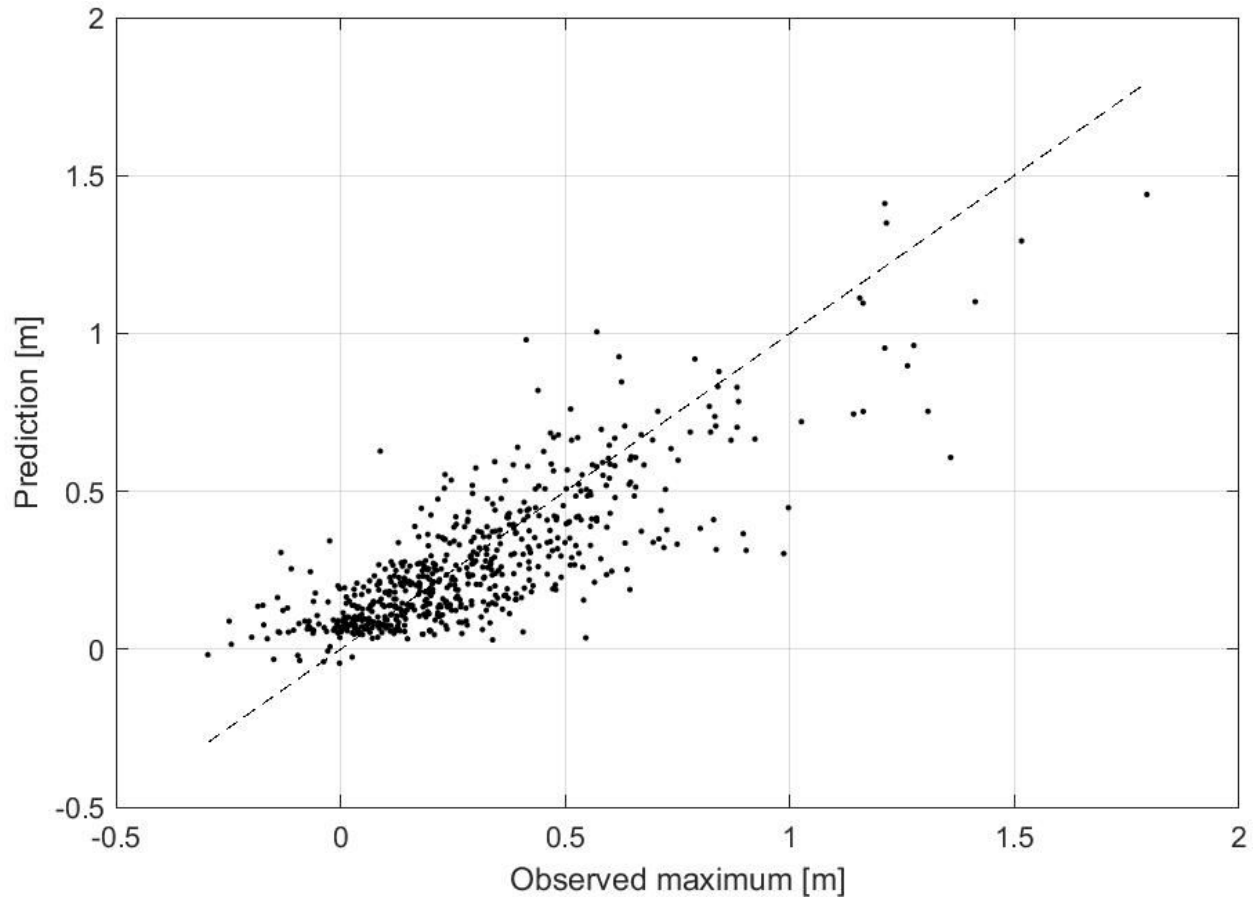


Figure 9: Observed and predicted storm surge maxima with best-fit line shown. Similar plots are available for storm minima, storm median and storm range.

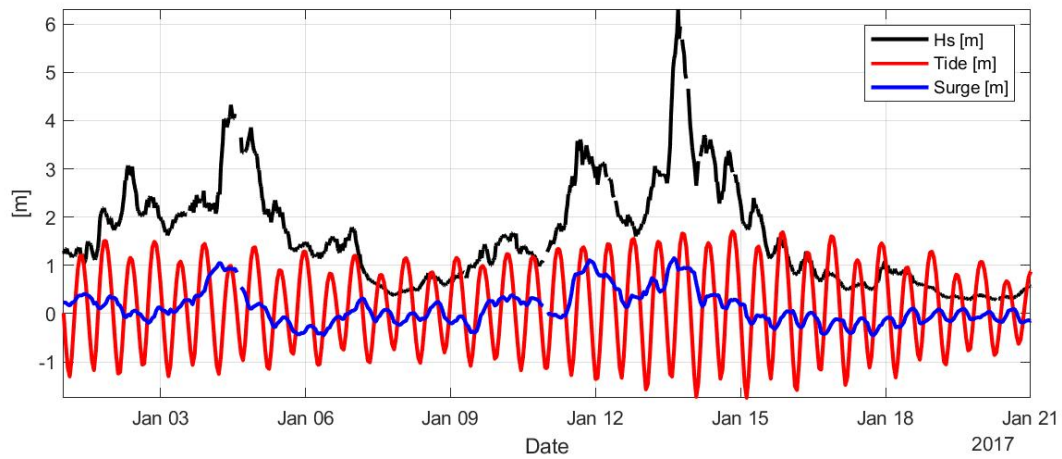


Figure 10: Time series of  $H_S$ , surge and tide for a shallow-water location (21.0m) showing the impact that tide can have on the variation in  $H_S$  through storms.

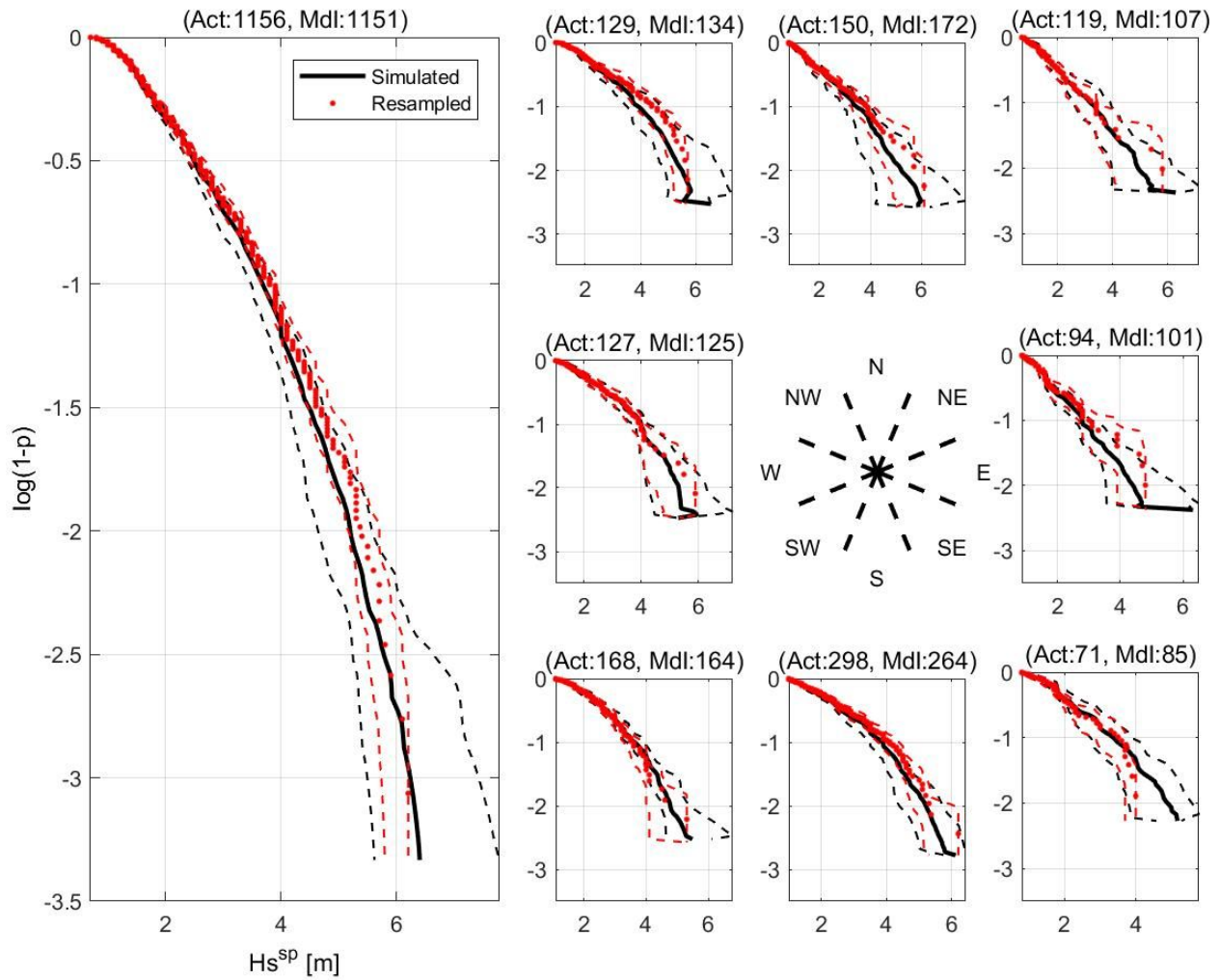


Figure 11: Comparison between resampled underlying data (red) and simulated (black) storm peaks for the overall case (left) and for each directional sector. Solid lines represent median case, dashed lines represent the 95% uncertainty intervals. The original data is shown as red dots. Similar plots are available resolved by month.

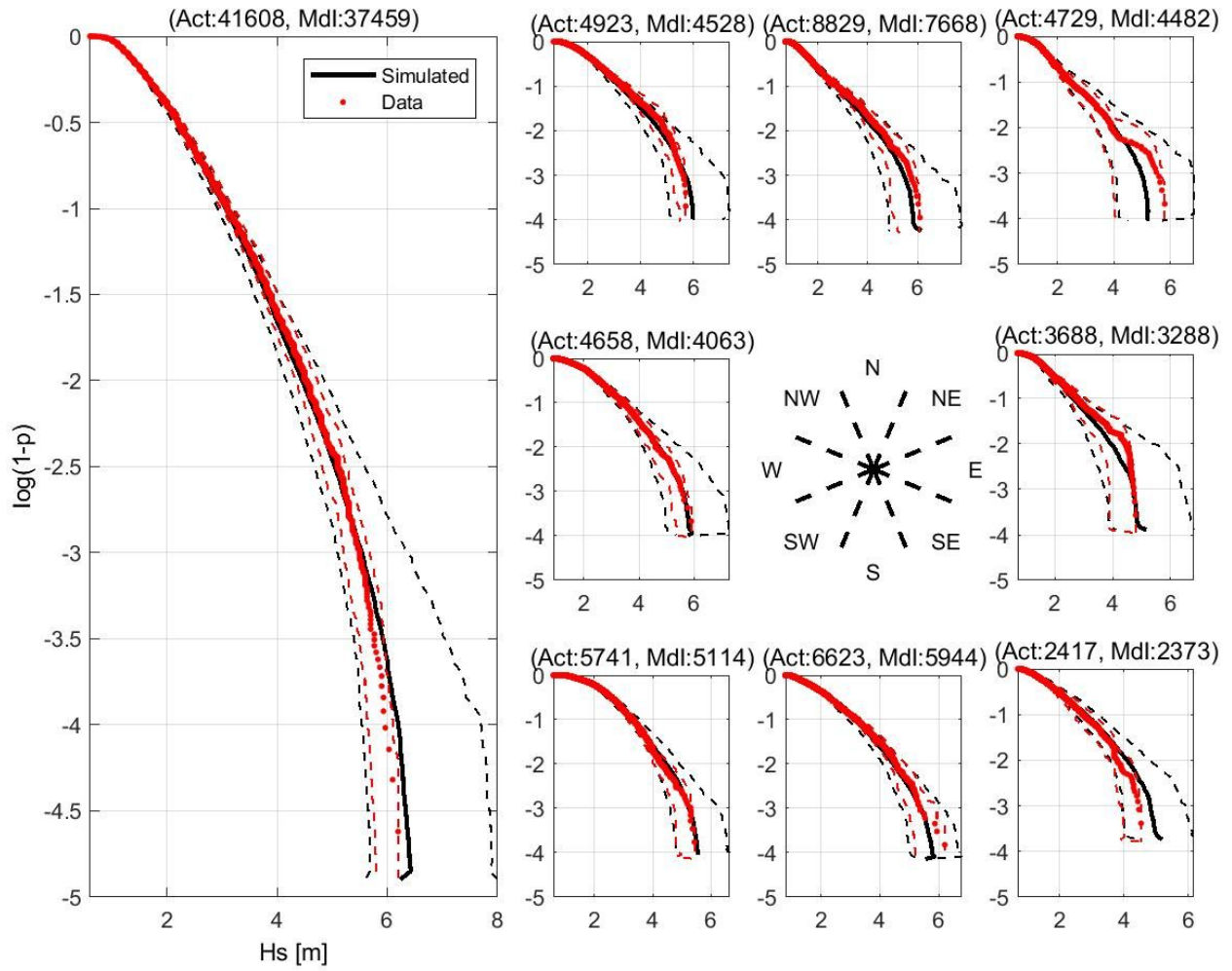


Figure 12: Comparison between resampled underlying data (red) and simulated (black) all storm sea-states for the overall case (left) and for each directional sector. Solid lines represent median case, dashed lines represent the 95% uncertainty intervals. The original data is shown as red dots. Similar plots are available resolved by month.

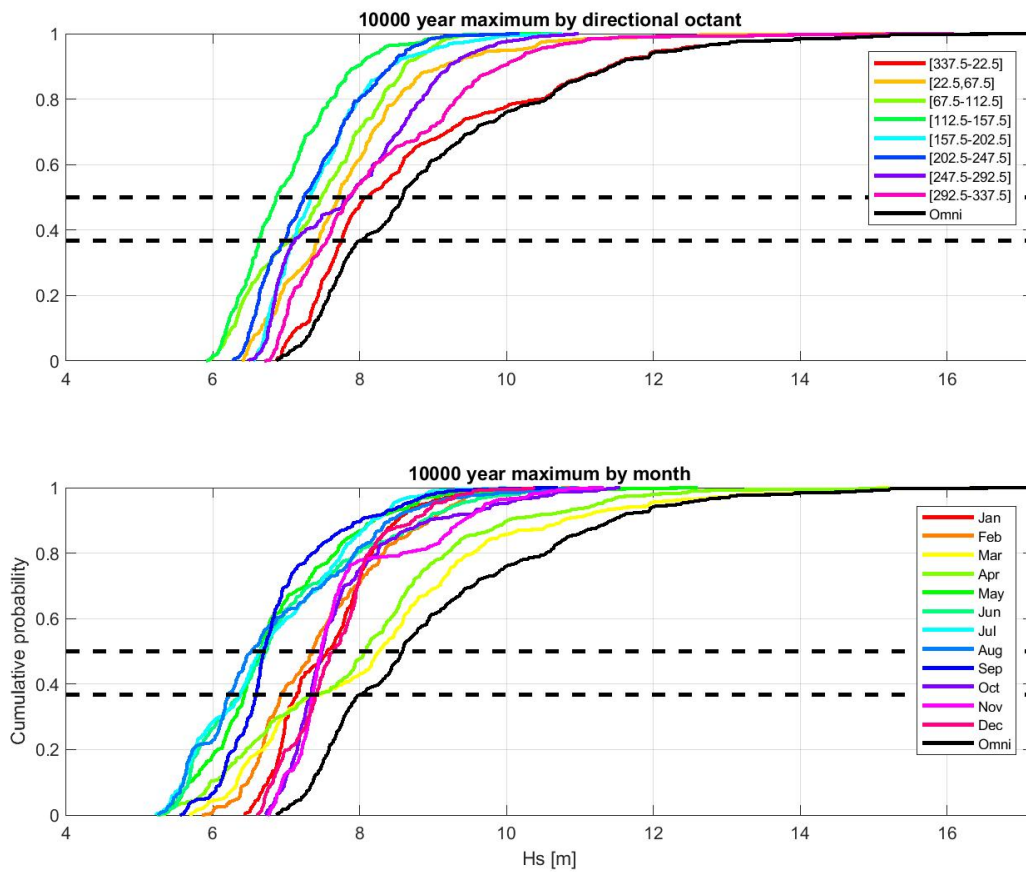


Figure 13: Distribution of the 10,000-year maximum of  $H_S$  (a) by direction and (b) by season. In each case, the overall *omni-covariate* curve is shown in black.

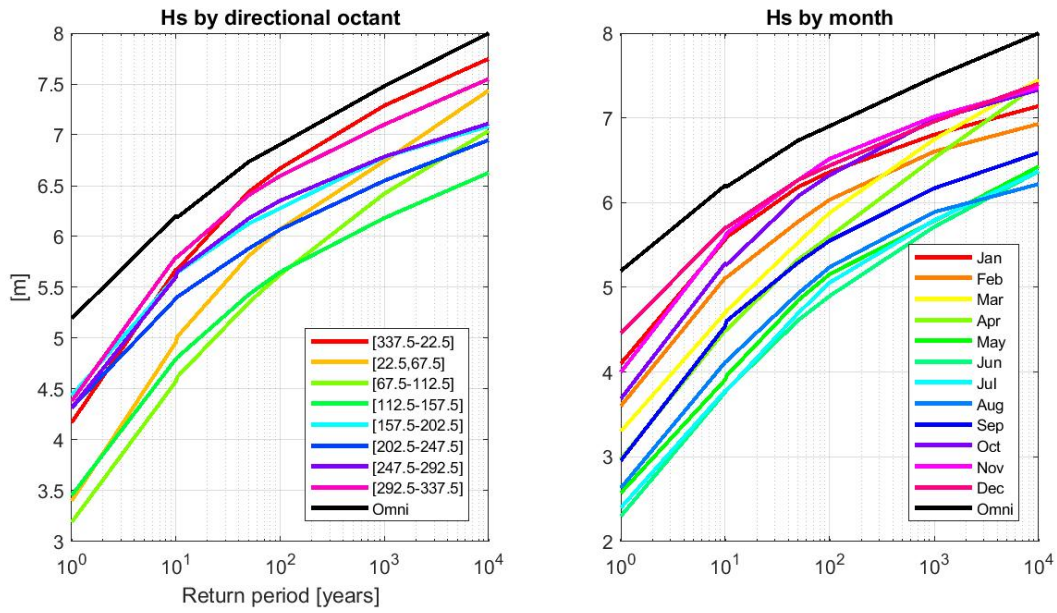


Figure 14: 37<sup>th</sup> percentile of the distribution of  $N$ -year maximum  $H_S$  (a) by direction and (b) by season, by return period. The overall omni-covariate curve is shown in black.

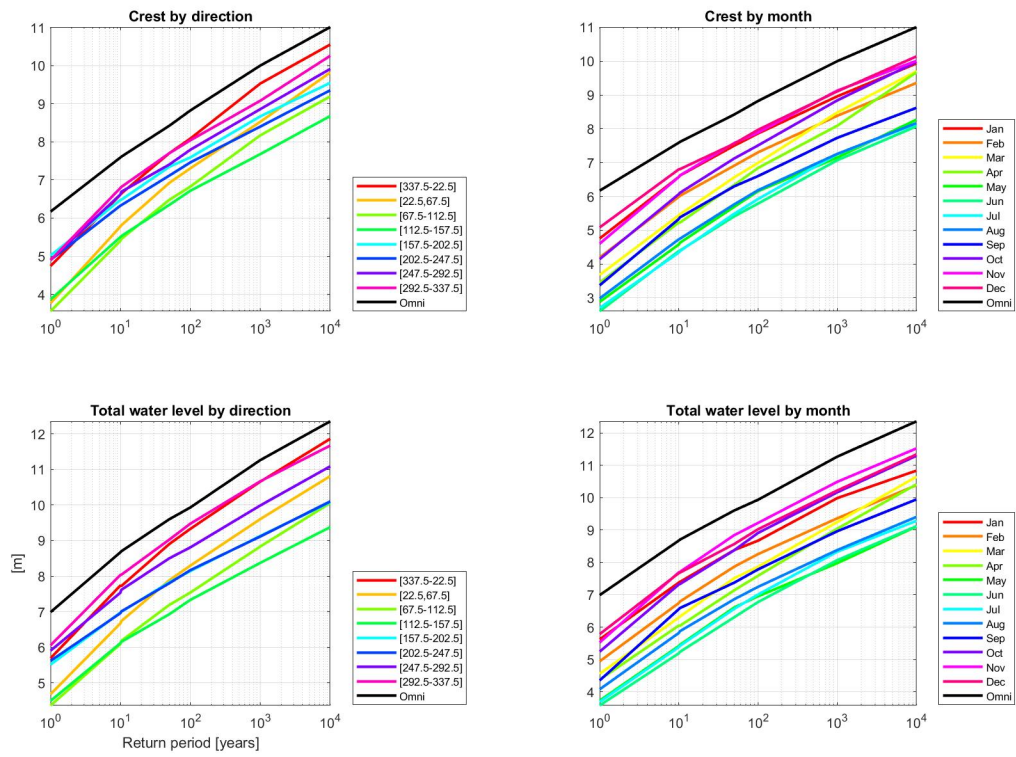


Figure 15:  $37^{th}$  percentile of the distribution for  $N$ -year maximum (a) wave crest by direction, (b) wave crest by season, (c) total water level by direction, and (d) total water level by season, as a function of return period. The overall omni-covariate curve is shown in black.



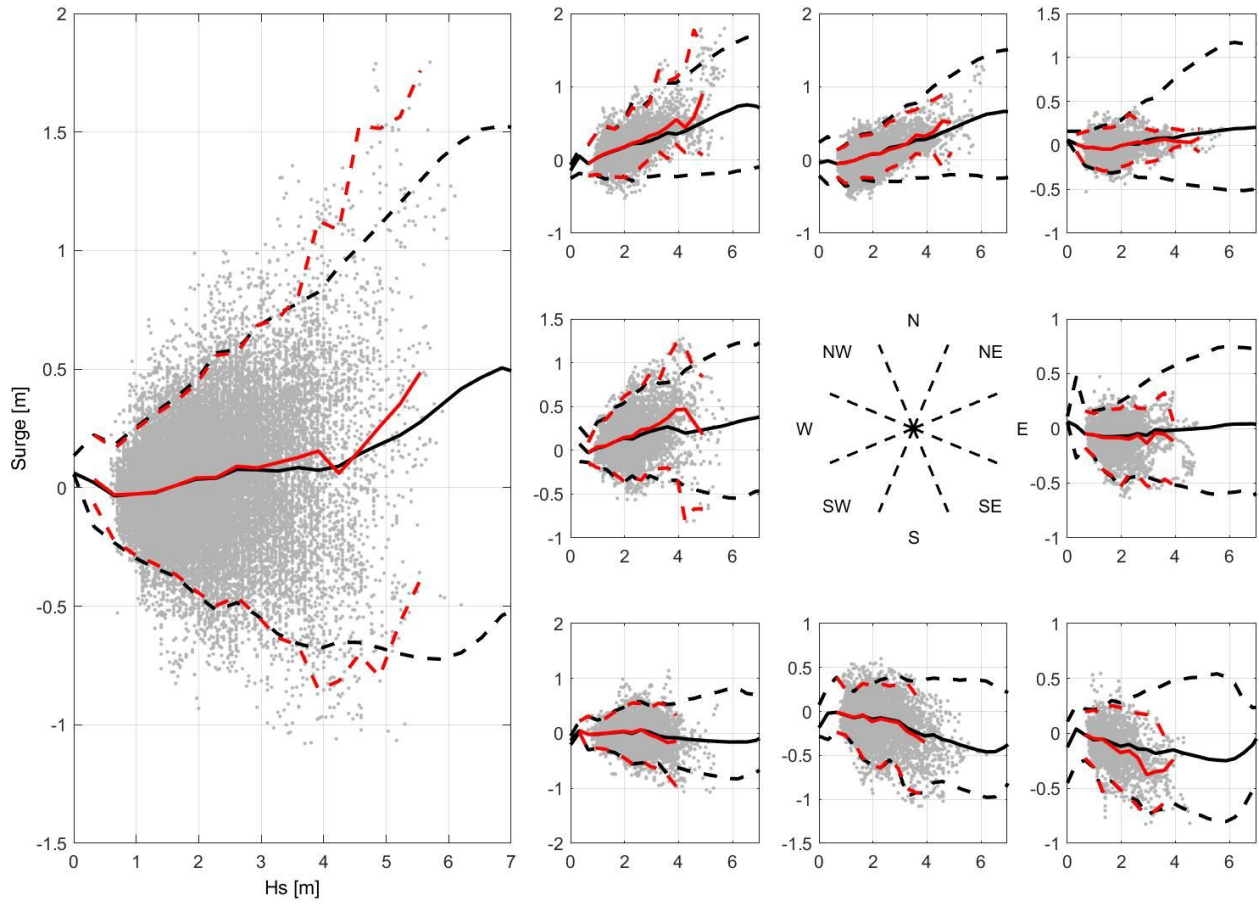


Figure 16: Comparison of observed (red) and simulated (black) median and 95% uncertainty intervals for storm surge versus  $H_S$ . Actual historical pairs of sea state  $H_S$  and surge are given as grey dots.

611 **List of Tables**

612	1	Estimates for the 37 <sup>th</sup> percentile of the distribution of the $N$ -year maximum wave crest (in metres) for 8 directional octants and omnidirectionally, as a function of return period. . . . .	35
613			
614			
615	2	Estimates for the 37 <sup>th</sup> percentile of the distribution of the $N$ -year maximum TWL (in metres) for 8 directional octants and omnidirectionally, as a function of return period. . . . .	36
616			
617			
618	3	Estimates for difference (in metres) between the 37 <sup>th</sup> percentile of the distribution of the $N$ -year maximum TWL and the 37 <sup>th</sup> percentile of the distribution of the $N$ -year maximum wave crest for 8 directional octants and omnidirectionally, as a function of return period. . . . .	37
619			
620			
621			
622	4	Estimates for the 37 <sup>th</sup> percentile of the distribution of the $N$ -year maximum wave crest (in metres) per month and all-year (over all months), as a function of return period. . . . .	38
623			
624			
625	5	Estimates for the 37 <sup>th</sup> percentile of the distribution of the $N$ -year maximum TWL (in metres) per month and all-year (over all months), as a function of return period. . . . .	39
626			
627	6	Estimates for difference (in metres) between the 37 <sup>th</sup> percentile of the distribution of the $N$ -year maximum TWL and the 37 <sup>th</sup> percentile of the distribution of the $N$ -year maximum wave crest per month and all-year (over all months), as a function of return period. . . . .	40
628			
629			
630			

Crest	Return Period [years]					
	1	10	50	100	1000	10000
<b>N</b>	4.7	6.6	7.7	8.1	9.5	10.6
<b>NE</b>	3.8	5.8	6.9	7.3	8.5	9.8
<b>E</b>	3.6	5.4	6.5	6.8	8.2	9.2
<b>SE</b>	3.9	5.5	6.3	6.7	7.7	8.7
<b>S</b>	5.0	6.5	7.3	7.6	8.7	9.5
<b>SW</b>	4.9	6.3	7.1	7.5	8.4	9.4
<b>W</b>	4.9	6.6	7.4	7.8	8.9	9.9
<b>NW</b>	4.9	6.8	7.7	8.0	9.1	10.3
<b>Omni</b>	6.2	7.6	8.4	8.8	10.0	11.0

Table 1: Estimates for the 37<sup>th</sup> percentile of the distribution of the  $N$ -year maximum wave crest (in metres) for 8 directional octants and omnidirectionally, as a function of return period.

TWL	Return Period [years]					
	1	10	50	100	1000	10000
<b>N</b>	5.7	7.7	8.9	9.3	10.7	11.9
<b>NE</b>	4.7	6.7	7.9	8.3	9.6	10.8
<b>E</b>	4.4	6.1	7.2	7.5	8.8	10.1
<b>SE</b>	4.5	6.1	6.9	7.3	8.4	9.4
<b>S</b>	5.5	7.0	7.8	8.1	9.1	10.1
<b>SW</b>	5.6	7.0	7.8	8.2	9.1	10.1
<b>W</b>	5.9	7.5	8.5	8.8	10.0	11.1
<b>NW</b>	6.1	8.0	9.0	9.5	10.7	11.7
<b>Omni</b>	7.0	8.7	9.6	9.9	11.3	12.4

Table 2: Estimates for the 37<sup>th</sup> percentile of the distribution of the  $N$ -year maximum TWL (in metres) for 8 directional octants and omnidirectionally, as a function of return period.

Implied SWL	Return Period [years]					
	1	10	50	100	1000	10000
<b>N</b>	0.9	1.1	1.2	1.2	1.1	1.3
<b>NE</b>	0.9	0.9	1.0	1.0	1.1	1.0
<b>E</b>	0.8	0.7	0.7	0.7	0.7	0.9
<b>SE</b>	0.6	0.6	0.6	0.6	0.7	0.7
<b>S</b>	0.5	0.5	0.5	0.6	0.5	0.5
<b>SW</b>	0.7	0.6	0.7	0.7	0.7	0.8
<b>W</b>	1.0	0.9	1.1	1.0	1.1	1.2
<b>NW</b>	1.2	1.2	1.3	1.4	1.6	1.4
<b>Omni</b>	0.8	1.1	1.2	1.1	1.3	1.4

Table 3: Estimates for difference (in metres) between the 37<sup>th</sup> percentile of the distribution of the  $N$ -year maximum TWL and the 37<sup>th</sup> percentile of the distribution of the  $N$ -year maximum wave crest for 8 directional octants and omnidirectionally, as a function of return period.

Crest	Return Period [years]					
	1	10	50	100	1000	10000
Jan	4.8	6.6	7.5	7.9	9.0	9.9
Feb	4.2	6.0	6.9	7.3	8.4	9.4
Mar	3.7	5.4	6.6	7.0	8.5	9.7
Apr	3.4	5.2	6.3	6.8	8.1	9.7
May	2.9	4.6	5.7	6.2	7.2	8.3
Jun	2.6	4.4	5.4	5.8	7.1	8.1
Jul	2.7	4.3	5.5	5.9	7.2	8.1
Aug	3.0	4.7	5.8	6.2	7.3	8.2
Sep	3.4	5.3	6.3	6.6	7.7	8.6
Oct	4.1	6.1	7.1	7.5	8.8	10.0
Nov	4.6	6.6	7.6	7.9	9.1	10.0
Dec	5.1	6.8	7.6	8.0	9.1	10.1
All Year	6.2	7.6	8.4	8.8	10.0	11.0

Table 4: Estimates for the 37<sup>th</sup> percentile of the distribution of the  $N$ -year maximum wave crest (in metres) per month and all-year (over all months), as a function of return period.

TWL	Return Period [years]					
	1	10	50	100	1000	10000
Jan	5.6	7.4	8.4	8.7	10.0	10.8
Feb	4.9	6.7	7.9	8.3	9.4	10.4
Mar	4.6	6.3	7.5	7.9	9.2	10.6
Apr	4.4	6.0	7.1	7.6	9.0	10.4
May	3.7	5.4	6.6	7.0	8.0	9.1
Jun	3.6	5.2	6.3	6.8	8.1	9.1
Jul	3.7	5.4	6.6	7.0	8.3	9.3
Aug	4.1	5.8	6.9	7.2	8.4	9.4
Sep	4.4	6.6	7.4	7.8	9.0	9.9
Oct	5.2	7.3	8.4	8.9	10.2	11.3
Nov	5.5	7.7	8.8	9.2	10.5	11.5
Dec	5.8	7.7	8.6	9.0	10.2	11.3
All Year	7.0	8.7	9.6	9.9	11.3	12.4

Table 5: Estimates for the 37<sup>th</sup> percentile of the distribution of the  $N$ -year maximum TWL (in metres) per month and all-year (over all months), as a function of return period.

Implied SWL	Return Period [years]					
	1	10	50	100	1000	10000
Jan	0.9	0.8	0.9	0.8	1.0	0.9
Feb	0.8	0.8	1.0	1.0	1.0	1.0
Mar	0.9	0.9	0.9	0.9	0.8	0.9
Apr	0.9	0.8	0.8	0.7	1.0	0.7
May	0.9	0.8	0.9	0.8	0.8	0.8
Jun	1.0	0.8	0.9	1.0	1.0	1.0
Jul	1.0	1.0	1.1	1.1	1.1	1.1
Aug	1.1	1.1	1.1	1.1	1.1	1.2
Sep	1.0	1.2	1.1	1.2	1.2	1.3
Oct	1.1	1.3	1.3	1.4	1.3	1.3
Nov	0.9	1.1	1.3	1.3	1.4	1.5
Dec	0.7	0.9	1.0	1.1	1.1	1.2
All Year	0.8	1.1	1.2	1.1	1.3	1.4

Table 6: Estimates for difference (in metres) between the 37<sup>th</sup> percentile of the distribution of the  $N$ -year maximum TWL and the 37<sup>th</sup> percentile of the distribution of the  $N$ -year maximum wave crest per month and all-year (over all months), as a function of return period.